Tracking Economic Activity With Alternative High-Frequency Data

Working Paper

Author(s):
Eckert, Florian; Kronenberg, Philipp; Mikosch, Heiner; Neuwirth, Stefan

Publication date:
2020-12

Permanent link:
https://doi.org/10.3929/ethz-b-000458723

Originally published in:
KOF Working Papers 488

ETH zürich

KOF Swiss Economic Institute

Tracking Economic Activity With Alternative High-Frequency Data

Florian Eckert, Philipp Kronenberg, Heiner Mikosch and Stefan Neuwirth

KOF Working Papers, No. 488, December 2020

KOF

KOF

ETH Zurich
KOF Swiss Economic Institute
LEE G 116
Leonhardstrasse 21
8092 Zurich, Switzerland

Phone +41 44 632 42 39
Fax +41 44 632 12 18
www.kof.ethz.ch
kof@kof.ethz.ch

Tracking Economic Activity With Alternative High-Frequency Data

Florian Eckert[†], Philipp Kronenberg[†], Heiner Mikosch[*†], and Stefan Neuwirth[†]

[†]KOF Swiss Economic Institute, ETH Zurich

December 16, 2020

Abstract

Most macroeconomic indicators failed to capture the sharp economic fluctuations during the Corona crisis in a timely manner. Instead, alternative high-frequency data have been used, aiming to monitor the economic situation. However, these data are often only loosely related to the business cycle and come with irregular patterns of missing observations, ragged edges and short histories. This paper presents a novel mixed-frequency dynamic factor model for measuring economic activity at high-frequency intervals in rich data environments. Previous research has estimated the dynamic factor conditional on actually observed data only. In contrast, we propose to estimate the dynamic factor conditional on a balanced panel with observed and latent data information, where the latent data are themselves estimated in a separate state-space block. One benefit of this data augmentation strategy is that it allows to easily account for serial correlation in the factor measurement errors. We apply the model to a set of daily, weekly, monthly and quarterly series and extract a dynamic factor, which is identified as the weekly growth rate of GDP. It turns out that the model is well suited to exploit the business cycle information contained in alternative high-frequency data. GDP is tracked timely and accurately during the Corona crisis and past economic crises.

JEL Classification: C11, C32, C38, C53, E32, E37

Keywords: Economic Activity Indicator, Real Time, Nowcasting, Alternative High-Frequency Data, Mixed-Frequency Dynamic Factor Model, Data Augmentation

[*]Corresponding author: ETH Zurich, Leonhardstrasse 21, Building LEE, 8092 Zurich, Switzerland, e-mail: mikosch@kof.ethz.ch, phone: +41 44 632 42 33, fax: +41 44 632 12 18

1 Introduction

The Corona crisis has shaken many economies worldwide to an unprecedented extent. Economic activity fell dramatically within a few days and rebounded very quickly after the first wave of lockdowns ended. Macroeconomic indicators, such as business tendency surveys, consumer sentiment, retail sales or industrial production, could not keep track of the sudden fluctuations. Most of these variables are released only once a month and with a publication lag, making them not well suited to capture the dynamics in a timely manner. Instead, business cycle observers started to use various high-frequency series such as daily credit card transactions, energy consumption, traffic volumes, smartphone mobility tracking and internet search hits, with the aim of monitoring economic activity closer to real time. Henceforth, we refer to these series as *alternative high-frequency data*, a term which is increasingly common since the outbreak of the crisis. However, the real-time monitoring task is challenging due to the characteristics of the alternative high-frequency data. Some of the series are only loosely related to economic activity as measured by statistical offices. Others cover only very specific aspects of economic activity. In addition, the series often fluctuate strongly and are affected by factors unrelated to the business cycle. Furthermore, most of them have only a short history and are subject to irregular patterns of missing observations and publication lags.

Against this background, we propose a novel mixed-frequency dynamic factor model (DFM) which is well suited to measure GDP growth at high-frequency intervals and close to real time and to extract the business cycle information contained in alternative high-frequency data, despite their aforementioned challenges. Our DFM accounts for stochastic volatility and for serial correlation in the factor measurement errors. It comprises three interdependent state-space blocks: latent high-frequency data, dynamic factor and stochastic volatility. In the first block, all unobserved data points in the mixed-frequency data set are estimated as latent states conditional on, among others, the actually observed data and temporal aggregation constraints. In the second block, the dynamic factor is estimated conditional on, amongst others, the observed as well as the estimated latent information. The strategy of creating a balanced data set through estimation of unobserved information as latent states is known as *data augmentation* in the statistics literature (Tanner and Wong, 1987; Frühwirth-Schnatter, 1994). We take a fully Bayesian approach to estimate the latent information, the dynamic factor, the stochastic volatility and all model parameters. The joint posterior is simulated using Gibbs sampling.

The literature on mixed-frequency DFMs has seen important advances during the past years (e.g., Giannone et al., 2008; Aruoba et al., 2009; Camacho and Perez-Quiros, 2010; Doz et al., 2011; Bańbura et al., 2011; Bańbura and Modugno, 2014). However, the handling of data sets with several mixed frequencies, with a large set of daily and weekly series, with arbitrary and irregular patterns of missing observations and with data histories of

varying lengths remains a challenge. Here, our paper provides several novel contributions. To begin with, previous models estimate the dynamic factor by modifying the Kalman filter recursions such that they skip the updating step if observations are missing. In contrast, our model estimates the dynamic factor not just based on actually observed data only, but also conditional on the *latent* information contained in the data set. For this, we integrate a novel state-space block into the DFM, in which the sparse observed data points in the mixed-frequency data set are augmented to a balanced panel with observed and estimated latent information. An important advantage of creating the balanced panel in the data augmentation block is that it allows for quasi-differencing of the dynamic factor measurement equation (Chib and Greenberg, 1994). Thereby, the model can easily account for serial correlation in the factor measurement errors despite mixed frequencies, missing observations, different release lags and data histories of various different lengths in the original data. This feature is crucial since it allows the common factor to have less explanatory power for the mixed-frequency series during extended periods of time while explaining a lot during other periods (e.g., Stock and Watson, 2002). This, in turn, can greatly improve the performance of DFMs, especially when alternative high-frequency data with the aforementioned characteristics are used. Previous papers obtain the conditional moments of the serially correlated measurement errrors from the Kalman smoother, typically using an EM-algorithm, which increases the computational burden substantially (e.g., Bańbura and Modugno, 2014). In contrast, we provide an efficient and generic Bayesian sampling algorithm that scales well to larger data sets. In order to estimate the latent high-frequency data, the dynamic factor and the stochastic volatility, we build on the precision sampler framework developed by Chan and Jeliazkov (2009). Our novel contribution here is to extend their procedure to the mixed-frequency case by integrating the temporal aggregation scheme originally proposed by Mariano and Murasawa (2003). This leads to substantial efficiency gains compared to forward filtering backward sampling (Carter and Kohn, 1994; Kim and Nelson, 2017), in particular when dealing with the large state-space setups required for mixed- and high-frequency data. Another advantage of our approach is that the dynamic factor resulting from the model estimation has a clear and intuitive interpretation. In particular, we propose straightforward identifying restrictions such that the common factor extracted from a mixed-frequency data set can be interpreted as the high-frequency period-on-period growth rate of GDP.

In an empirical application, we study how useful the DFM is for tracking Swiss GDP with a large set of daily, weekly and monthly time series, including various alternative high-frequency data. We derive a weekly economic activity indicator that is identified as week-on-week GDP growth. A pseudo real-time analysis yields that the indicator is able to capture business cycle turning points comparatively early. It tracks economic activity well during times of sudden and strong economic fluctuations such as the Great Recession in 2008/09, the European sovereign debt crisis in 2011 and the Swiss franc shock in 2015. An in-depth investigation is provided for the Corona crisis, where the weekly GDP

indicator performs especially well due to the information extracted from the alternative high-frequency data.[1] Further, we conduct a pseudo real-time out-of-sample nowcast exercise for quarterly GDP. The mixed-frequency DFM substantially outperforms simple benchmark models. The alternative high-frequency data turn out to be especially useful for nowcasting GDP during sharp economic downturns and recoveries as compared to using macroeconomic and financial series only. In contrast, the alternative high-frequency data do not provide additional valuable information during normal times.

The remainder of the paper is structured as follows. Section 2 presents the mixed-frequency DFM with stochastic volatility, where special emphasis is put on the discussion of the data augmentation part. The section further describes the identifying assumptions and discusses our estimation priors. In addition, a description of the sampling algorithm is provided. Section 3 presents the results from the empirical application, including a description of the employed data. Section 4 concludes.

2 Mixed-Frequency DFM with Data Augmentation

2.1 Data Augmentation

The model uses a collection of n time series with mixed frequencies, where the time index of the highest frequency in the data set is denoted by t. In order to coerce all time series to the highest frequency, low-frequency observations are registered in the last high-frequency entry of the corresponding low-frequency period and all other entries are filled with zeros. For instance, when mixing weekly, monthly and quarterly data, monthly (quarterly) data are observed in the last week of each month (quarter) and are set to zero elsewhere. A time series is also assigned a value of zero in a period if the observation is missing due to publication delays or a limited history. The n-dimensional data vector $\mathbf{y}_t$ is, therefore, typically filled with a few observations and many zeros. Further, we define $\mathbf{x}_t$ as an n-dimensional vector filled with actual observations and with estimated latent observations whenever a variable is not observed. The relation between the sparse vector $\mathbf{y}_t$ and the dense vector $\mathbf{x}_t$ is described by the following identity:

$$\mathbf{y}_t = \mathbf{S}_t \mathbf{x}_t, \tag{1}$$

where $\mathbf{S}_t$ is a diagonal selection matrix of order $n \times n$, featuring ones on the diagonal if the corresponding value in $\mathbf{y}_t$ is observed and zeros otherwise. Henceforth, we refer to the strategy of augmenting the sparse vector $\mathbf{y}_t$ to the dense vector $\mathbf{x}_t$, which contains observed and estimated data, as data augmentation. Consequently, Equation (1) is referred to as

[1] We would like to highlight other recent projects that employ alternative high-frequency data to track the economy during the Corona crisis. Lewis et al. (2020) provide a weekly economic activity indicator for the United States using both a principal components and a dynamic factor approach. Eraslan and Götz (2020) do so for Germany taking a principal components approach. For Switzerland, Eckert and Mikosch (2020) present daily activity indicators and Guggia et al. (2020) present a weekly economic activity index.

the *data augmentation equation.* As will be seen in the next subsection, data augmentation enables us to easily account for serial correlation in the measurement errors of a mixed-frequency DFM.

2.2 Dynamic Factor

The *measurement equation for the dynamic factor* f_t is given by

$$\mathbf{x}_t = \mathbf{L}_0\boldsymbol{\lambda}f_t + \mathbf{L}_1\boldsymbol{\lambda}f_{t-1} + \ldots + \mathbf{L}_s\boldsymbol{\lambda}f_{t-s} + \mathbf{e}_t. \tag{2}$$

where s indicates the number of factor lags, the n-dimensional vector $\boldsymbol{\lambda}$ contains the time-invariant factor loadings and the diagonal distributed lag matrices $\mathbf{L}_0, \ldots, \mathbf{L}_s$ ensure the appropriate temporal aggregation of the high-frequency factor to the lower frequency variables in $\mathbf{x}_t$, as proposed by Mariano and Murasawa (2003) (see Appendix A.1 for details). The measurement errors in Equation (2) follow the first-order autoregressive process

$$\mathbf{e}_t = \boldsymbol{\rho}\mathbf{e}_{t-1} + \mathbf{u}_t \qquad \mathbf{u}_t \sim \mathcal{N}(\mathbf{0}, \boldsymbol{\Sigma}) \tag{3}$$

with the error covariance matrix $\boldsymbol{\Sigma}$ and the autoregressive coefficient matrix $\boldsymbol{\rho}$ being diagonal. In order to estimate the dynamic factor in presence of serial correlation in the measurement errors, we follow Chib and Greenberg (1994) and quasi-difference the measurement equation. For this, we first define the quasi-differenced augmented data vector as

$$\tilde{\mathbf{x}}_t = \mathbf{x}_t - \boldsymbol{\rho}\mathbf{x}_{t-1}. \tag{4}$$

Inserting Equation (2) into Equation (4) yields the *quasi-differenced measurement equation for the dynamic factor*:

$$\tilde{\mathbf{x}}_t = \Big(\mathbf{L}_0\boldsymbol{\lambda}f_t + \ldots + \mathbf{L}_s\boldsymbol{\lambda}f_{t-s}\Big) - \boldsymbol{\rho}\Big(\mathbf{L}_0\boldsymbol{\lambda}f_{t-1} + \ldots + \mathbf{L}_s\boldsymbol{\lambda}f_{t-s-1}\Big) + \mathbf{u}_t, \tag{5}$$

where $\mathbf{u}_t$ has been defined in Equation (3) and is serially uncorrelated.[2] Notably, the elimination of serially correlated measurement errors via quasi-differencing is only possible because the original measurement equation given in Equation (2) includes the dense data vector $\mathbf{x}_t$. In contrast, elimination of serially correlated measurement errors by quasi-differencing is not possible when the measurement equation includes the sparse data vector $\mathbf{y}_t$. Thus, the data augmentation from $\mathbf{y}_t$ to $\mathbf{x}_t$ is a necessary step to account for serial correlation in the measurement errors. The *state equation for the dynamic factor* is given by the autoregressive process

$$f_t = \phi_1 f_{t-1} + \ldots + \phi_p f_{t-p} + e^{h_t}\eta_t, \qquad \eta_t \sim \mathcal{N}(0, 1) \tag{6}$$

[2]It is straightforward to rearrange terms in Equation (5) to simplify the estimation of the factor.

where the scalars $\phi_1, \ldots, \phi_p$ represent the autoregressive coefficents and p indicates the number of lags. The composite error term $e^{h_t}\eta_t$ consists of the time-varying stochastic volatility factor e^{h_t} and the standard normally distributed error η_t. Note that the state equation is not affected by the transformation from the original to the quasi-differenced measurement equation. Also, this transformation does not affect the measurement and the state equation for the stochastic volatility discussed in the next section.

2.3 Stochastic Volatility

We let the variance of the error term in Equation (6) be time varying in order to better capture volatility increases during crisis periods. Specifically, the logarithmized stochastic volatility factor follows the random walk process

$$h_t = h_{t-1} + v_t, \qquad v_t \sim \mathcal{N}(0, \omega) \tag{7}$$

which gives us the *state equation of the stochastic volatility factor*. Since solving Equation (6) for h_t would result in nonlinearities, we follow Primiceri (2005) and transform the equation to a linear system by squaring and taking logarithms. This results in the following *measurement equation for the stochastic volatility factor*:

$$\log\Big((f_t - \phi_1 f_{t-1} - \ldots - \phi_p f_{t-p})^2 + c\Big) = 2h_t + \log\left(\eta_t^2\right), \tag{8}$$

where the offset constant $c = 0.001$ is introduced to make the estimation more robust. Since η_t follows a standard normal distribution, the error term $\log\left(\eta_t^2\right)$ is distributed according to a log chi-squared distribution with one degree of freedom, $\log\chi^2(1)$. In order to transform the system further to a Gaussian state-space model, the $\chi^2(1)$-distribution is approximated using a mixture of normals following Kim et al. (1998). Appendix A.2 provides further details.

2.4 Latent Data

The *measurement equation for the latent dense data vector* $\mathbf{x}_t$ is given by

$$\mathbf{y}_t = \mathbf{S}_t\mathbf{x}_t + \boldsymbol{\epsilon}_t, \qquad \boldsymbol{\epsilon}_t \sim \mathcal{N}(0, \epsilon\mathbf{I}_n), \tag{9}$$

where $\epsilon = 10^{-9}$ is a very small number. This approximates the identity given in Equation (1) very closely. Imposing an exact identity is not feasible, as the covariance matrix needs to be invertible in the precision sampling approach that we employ for estimation. The *state equation for* $\mathbf{x}_t$ is simply obtained by combining Equation (5) and Equation (4) to

$$\mathbf{x}_t = \Big(\mathbf{L}_0\boldsymbol{\lambda}f_t + \ldots + \mathbf{L}_s\boldsymbol{\lambda}f_{t-s}\Big) - \boldsymbol{\rho}\Big(\mathbf{L}_0\boldsymbol{\lambda}f_{t-1} + \ldots + \mathbf{L}_s\boldsymbol{\lambda}f_{t-s-1}\Big) + \boldsymbol{\rho}\mathbf{x}_{t-1} + \mathbf{u}_t, \tag{10}$$

where again $\mathbf{u}_t \sim \mathcal{N}(\mathbf{0}, \boldsymbol{\Sigma})$.

2.5 Factor Identification and Interpretation

Since both the dynamic factor and the factor loadings are unknown, there exist infinite possibilities to explain the data. This is commonly referred to as observational equivalence. Therefore, in order to identify the factor, certain restrictions have to be placed on the parameter space. Following Bai and Wang (2015), the factor loading on GDP, denoted as λ_{gdp}, is restricted to unity using informative priors. This resolves the scale and sign indeterminacy inherent in dynamic factor models. Rotational indeterminacy is not an issue in the single factor case (see, e.g., Aßmann et al., 2016, and references therein) and the dynamic factor is, therefore, uniquely identified.

One benefit of our approach is a clear and intuitive interpretation of the dynamic factor. This is achieved by imposing informative priors such that the dynamic factor is equal to the high-frequency growth rate of GDP and that the temporal aggregation of the dynamic factor, given in Equation (2), approximates the quarterly growth rate of GDP. Specifically, we shrink the autoregressive coefficient ρ_{gdp} strongly towards zero. In addition, we shrink the error term σ_{gdp} on GDP growth towards a small value. This value determines how much the temporally aggregated high-frequency factor is allowed to deviate from the observed GDP growth rates. It should be noted, that the shrinkage is neither necessary to achieve identification nor is it in any way inherent to our model itself. Other choices are possible depending on what the researcher wants to do with the model.

The priors on all remaining parameters are left completely uninformative. It leads to a more robust convergence, especially around turning points, when imposing additional stationarity constraints on the autoregressive coefficients of the dynamic factor. A detailed account of the conditional distributions is given in Appendix A.5.

2.6 Estimation

The estimation task comprises the estimation of the dynamic factor f_t, the stochastic volatility factor h_t, the latent dense data vector $\mathbf{x}_t$ as well as the parameters $\boldsymbol{\lambda}, \phi_1, \ldots, \phi_p$, $\boldsymbol{\rho}$, ω and $\boldsymbol{\Sigma}$. The joint posterior distribution is simulated using Gibbs sampling. f_t, h_t, $\mathbf{x}_t$ and the aforementioned parameters are estimated in separate Gibbs sampling blocks, conditional on the observed data $\mathbf{y}_t$, the selection matrix $\mathbf{S}_t$ and the distributed lag matrices $\mathbf{L}_0, \ldots, \mathbf{L}_s$. Sparse matrix preallocation and the use of sparse matrix algorithms make the estimation computationally efficient. A set of starting values is randomly generated from uniform distributions to ensure robust convergence of the sampler. We assess convergence of the Gibbs sampling algorithm using trace plots and by checking differences in the recursive means of selected parameters. Due to the parsimonious parameterization, a burn-in of 1,000 iterations is sufficient to achieve convergence. After convergence is achieved, another 1,000 draws are saved and evaluated.

For the estimation of f_t, h_t, $\mathbf{x}_t$ in the separate Gibbs sampling blocks, we build on the procedure proposed by Chan and Jeliazkov (2009). We extend the algorithm to the case of mixed-frequency data by integrating the temporal aggregation scheme of Mariano and Murasawa (2003) into the procedure. The rest of this section explains the estimation of f_t, while Appendices A.3, A.4 and A.5 describe the estimation h_t, $\mathbf{x}_t$ and the remaining parameters $\boldsymbol{\lambda}, \phi_1, \ldots, \phi_p, \omega, \boldsymbol{\rho}$ and $\boldsymbol{\Sigma}$, respectively.

To estimate f_t, the measurement equation for the factor shown in Equation (5) is stacked over all time periods $t = 1, \ldots, T$ to get

$$\tilde{\mathbf{x}} = \mathbf{G}\mathbf{f} + \mathbf{u}, \qquad \mathbf{u} \sim \mathcal{N}(\mathbf{0}, \mathbf{I}_T \otimes \boldsymbol{\Sigma}) \tag{11}$$

where

$$\underset{n(T-1)\times 1}{\tilde{\mathbf{x}}} = \begin{bmatrix} \tilde{\mathbf{x}}_2 \\ \vdots \\ \tilde{\mathbf{x}}_T \end{bmatrix}, \qquad \underset{n(T-1)\times(T+s)}{\mathbf{G}} =$$

$$\begin{bmatrix} -\boldsymbol{\rho}\mathbf{L}_s\boldsymbol{\lambda} & (\mathbf{L}_s - \boldsymbol{\rho}\mathbf{L}_{s-1})\boldsymbol{\lambda} & \ldots & (\mathbf{L}_1 - \boldsymbol{\rho}\mathbf{L}_0)\boldsymbol{\lambda} & \mathbf{L}_0\boldsymbol{\lambda} & \\ & \ddots & & \ddots & & \\ & -\boldsymbol{\rho}\mathbf{L}_s\boldsymbol{\lambda} & (\mathbf{L}_s - \boldsymbol{\rho}\mathbf{L}_{s-1})\boldsymbol{\lambda} & \ldots & (\mathbf{L}_1 - \boldsymbol{\rho}\mathbf{L}_0)\boldsymbol{\lambda} & \mathbf{L}_0\boldsymbol{\lambda} \end{bmatrix}.$$

Note that G integrates the temporal aggregation scheme of Mariano and Murasawa (2003) into the procedure of Chan and Jeliazkov (2009). The state equation for the factor given in Equation (6) is stacked correspondingly:

$$\mathbf{H}\mathbf{f} = \mathbf{v}, \qquad \mathbf{v} \sim \mathcal{N}(\mathbf{0}, \mathbf{V}) \tag{12}$$

where

$$\underset{(T+s)\times(T+s)}{\mathbf{H}} = \begin{bmatrix} 1 & & & & & \\ -\phi_1 & 1 & & & & \\ \vdots & \ddots & \ddots & & & \\ -\phi_p & \ldots & -\phi_1 & 1 & & \\ & \ddots & \ddots & \ddots & \ddots & \\ & & -\phi_p & \ldots & -\phi_1 & 1 \end{bmatrix}, \qquad \underset{(T+s)\times 1}{\mathbf{f}} = \begin{bmatrix} f_{1-s} \\ f_{2-s} \\ \vdots \\ f_1 \\ \vdots \\ f_T \end{bmatrix},$$

and $\mathbf{V}$ is a diagonal matrix containing the time-varying variances $e^{2h_{1-s}}, \ldots, e^{2h_T}$. The precision matrix $\mathbf{F}_0$ is then given by $\mathbf{H}'\mathbf{V}^{-1}\mathbf{H}$ and the conditional posterior of the factors

is normally distributed according to

$$\mathbf{f} \sim \mathcal{N}(\mathbf{f}_1, \mathbf{F}_1) \quad \text{where} \quad \mathbf{f}_1 = \mathbf{F}_1 \left(\mathbf{G}'(\mathbf{I}_T \otimes \mathbf{\Sigma}^{-1})\tilde{\mathbf{x}} \right)$$
$$\mathbf{F}_1 = \left(\mathbf{F}_0 + \mathbf{G}'(\mathbf{I}_T \otimes \mathbf{\Sigma}^{-1})\mathbf{G} \right)^{-1}.$$

This algorithm is computationally very efficient if block-banded matrix algorithms are used. Instead of inverting $\mathbf{F}_1$, it is faster to compute the banded Cholesky factor of $\mathbf{F}_1$ and to solve for $\mathbf{f}_1$ by forward and backward substitution.

3 Tracking GDP with Alternative High-Frequency Data

We want to know whether the mixed-frequency DFM is helpful for tracking economic activity. Our conjecture is that the model can be particularly useful during downturns and upturns, especially if they are very sharp as during the Corona crisis. For an empirical application, we assemble a set of mixed-frequency data on the Swiss economy and study the behavior of a weekly GDP indicator resulting from our model. Thereafter, we present a pseudo real time out-of-sample nowcast exercise for quarterly GDP growth.

3.1 Data

The employed data set includes 22 daily and one weekly series that can be classified as alternative high-frequency data. These data comprise diverse series such as, e.g., energy production and energy consumption volumes, the frequency of motor vehicles passing at important monitoring stations, the number of flight arrivals and departures at the main national airport, debit and credit card transaction volumes in retail trade, the volume of cash withdrawals at ATM machines, and google search hits for the economic situation and for the purchase of consumption goods. A general challenge with alternative high-frequency data is that their history is often quite short. In fact, some of our series start in 2018 only or even later. Our model can easily deal with data sets where the series start at different dates or at a late stage during the nowcasting analysis. The reason is that each series is a latent process in vector $\mathbf{x}_t$ of Equation (1), irrespectively of whether it is observed or not.

In addition to the alternative high-frequency series, the data set includes six daily and one monthly financial series as well as 23 monthly macroeconomic series (labor market, price, retail sale and business tendency survey variables). The set of financial and macroeconomic variables is rather standard in the GDP nowcasting literature. We are interested in knowing whether the alternative high-frequency data provide valuable information in addition to the standard variables. Table 2 in Appendix A.6 provides an overview of all series used in this paper, along with meta information such as frequency, starting date, unit, transformation and source. Since our nowcasting exercise is conducted at a weekly frequency, we aggregate all daily series in the data set to weekly frequency. A positive

side effect of the temporal aggregation is that weekly seasonality patterns in the daily series are circumvented. In order to ensure a regular frequency pattern of the time series, the aggregation is done such that each of the 12 months in a year consists of exactly four weekly observations, resulting in 48 weekly observations per year.

We carefully track the release dates of the weekly and monthly time series according to their release schedules of the year 2020. For the below real time analysis, only those observations, which were actually available at a particular date, are employed as an input for the model. Table 2 reports the release lags of all variables in the data set. The weekly variables are released in the following week. The monthly variables are released in the first week of the following month, except the retail sales variables which get published with a delay of four weeks. Quarterly GDP is released with a lag of 9 weeks. The variable-specific release lags result in "ragged edges" in the data (Wallis, 1986), which our model can easily deal with.

Figure 11 in Appendix A.6 shows our target variable, the quarter-on-quarter growth rate of Swiss real GDP, adjusted for financial inflows and outflows stemming from international sport events. Since the year 2005, the Swiss economy has experienced four economic crises: the Great Recession in 2008Q4–2009Q3, the European sovereign debt crisis in 2011Q3–2013Q1, the Swiss franc shock in 2015Q1–2015Q2, and the Corona crisis in 2020Q1–2020Q2.[3] It is debatable when exactly these crises started and ended. We simply choose the start and end periods of the crises such that they began with strong downturns of quarterly GDP and ended with strong upturns.

3.2 Weekly GDP Indicator

The dynamic factor resulting from our mixed-frequency DFM is constructed such that it approximately represents the annualized week-on-week growth rate of GDP (see Section 2.5). For this reason, we henceforth refer to the dynamic factor as *weekly GDP indicator*. The upper panel of Figure 1 shows the weekly indicator and its 95%-confidence interval. It is shown together with the actual quarter-on-quarter growth rate of GDP, indicated by horizontal red bars.[4] The weekly indicator and the quarter-on-quarter growth rate of GDP match well for the entire history. The lower panel shows the stochastic volatility of the errors in the state equation for the dynamic factor (see Equation (6)). Time-varying errors allow the factor to account for the higher volatility of economic activity during crisis periods. Indeed, we observe that the model makes use of this flexibility during periods of sudden and strong economic fluctuations, where the volatility of the error term increases.

[3] Note to the editors and referees: 2020Q3 had not yet been published when the empirical part of the paper was finalized. We are happy to include the continuation of the Corona crisis in a revised paper version.

[4] The unprecedented fluctuations during the Corona crisis eclipse the usual trajectory of weekly economic activity. We cropped the vertical axis of the figure to allow for an inspection of the fluctuations during other times. The Corona crisis will be discussed in greater detail later on.

Figure 1: History of Weekly GDP Growth and Stochastic Volatility. The upper panel shows the dynamic factor, representing the annualized week-on-week growth rate of Swiss real GDP, together with a 95%-confidence interval in blue. The red bars depict the official annualized quarter-on-quarter growth rate of real GDP. The lower panel shows the estimated stochastic volatility. Periods classified as economic crisis are indicated by vertical grey bars. The vertical axis of the upper panel is truncated to allow for an appropriate assessment of the entire history.

We conjecture that the previously presented alternative high-frequency data are especially useful in times of sharp and strong downturns and rebounds. They should capture the increased volatility faster and to a greater extent than traditional macroeconomic data. To study this, we now put a special emphasis on the four economic crises in Switzerland since the year 2005. We want to know whether the weekly GDP indicator is indeed able to capture these sudden and strong economic fluctuations. Figure 2 presents the close-up view of the weekly indicator together with 95%-confidence intervals (in blue) and with the realized annualized quarter-on-quarter growth rate of GDP (in red). The crisis quarters are indicated with vertical grey bars. During the Great Recession, the indicator shows negative growth rates already at the beginning of August 2008, with a trough in mid-November. From March 2009 onward, weekly growth turned positive again. The path of the weekly growth rates reveals that both the downturn and the subsequent recovery were very strong and abrupt, which cannot be captured by looking at quarterly or monthly figures only. During the European sovereign debt crisis, Switzerland experienced heightened volatility over several quarters due to an appreciation of the Swiss franc, increased uncertainty and very volatile transit trade. The weekly GDP indicator captures these ups and

downs quite well (see middle panel of Figure 2). On January 15, 2015, the Swiss National Bank unexpectedly removed the minimum exchange rate of 1.20 Swiss francs per euro. This led to a rapid appreciation of the Swiss franc, which has become known as the "Swiss franc shock". GDP declined by 0.7 percent in 2015Q1 and grew strongly again by 2.7 percent in the subsequent quarter. The weekly GDP indicator reveals that the economic downturn after the shock was relatively strong, but that a steep recovery started at the end of February already (see right panel of Figure 2). This prevented a more negative growth rate for 2015Q1. The indicator further reveals that economic activity was rather flat on average over the second quarter and that the strong quarterly growth rate was primarily due to a big statistical overhang stemming from the first quarter. Altogether, the analysis shows that the weekly GDP indicator can help to better understand rapid economic fluctuations after shocks.

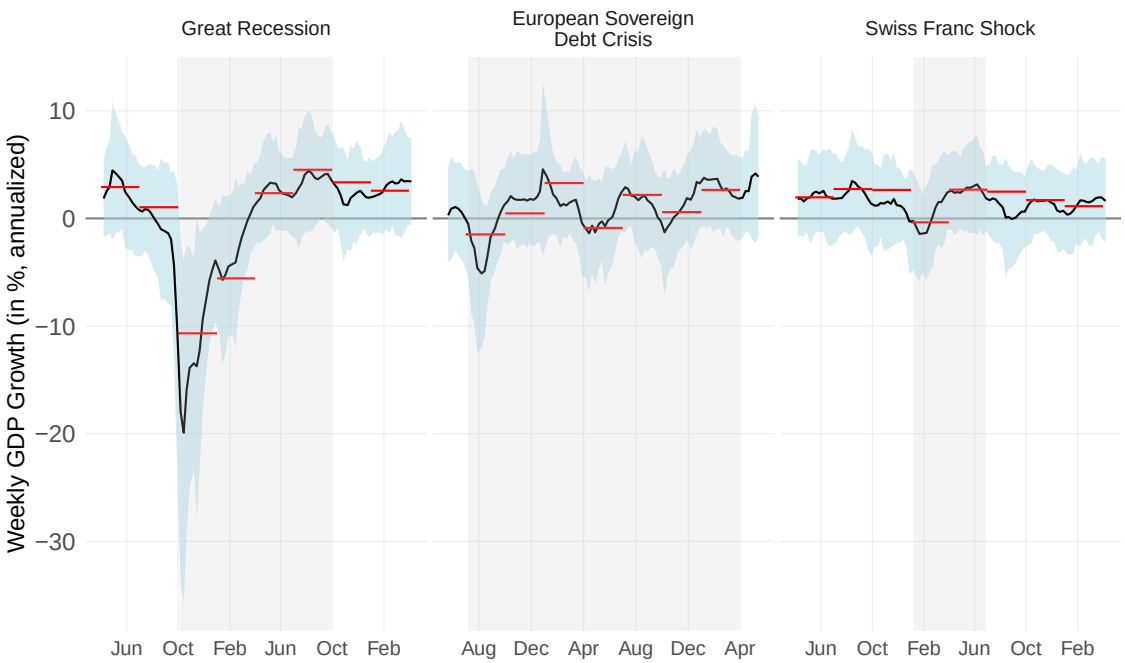

Figure 2: Weekly GDP Growth During Crisis Periods. Notes: See Figure 1.

Next, we focus on the Corona crisis during which the Swiss economy, just as other economies worldwide, experienced unprecedented fluctuations both in terms of suddenness and strength. Figure 3 shows the weekly GDP indicator, again together with a 95%-confidence interval and with the actual quarter-on-quarter growth rate of GDP. The vertical dotted lines indicate important policy decisions during the pandemic. The first Corona virus infection was recorded on February 25, 2020. Restrictions for events and gatherings of persons were increased stepwise during late February and early March. On March 16 the government eventually introduced a nationwide lockdown as the virus had spread throughout the country. The weekly GDP indicator reveals that economic activity had already decreased substantially before the lockdown. The reason for this is that

the population reduced its mobility and consumption activity already from late February onward as a reaction to the spread of the pandemic (e.g., Eckert and Mikosch, 2020). Firms cut down production which was also reflected in, e.g., a record increase of claims for short-term work. The lockdown pushed growth further into negative territory, reaching its low at the end of March with weekly annualized growth rates of around -120 percent. Infections numbers fell rapidly in April, public life restarted in turn and stores as well as schools reopened on April 29. This led to a rapid rebound with weekly growth rates of nearly the similar absolute magnitude as during the previous decline. Since May, weekly GDP growth gradually returned to "normal" rates reaching around 2 percent in September. An important policy lesson is that economic activity dropped not only due to the lockdown imposed by the government. Rather, growth fell into negative territory already before the lockdown, as consumers and producers reduced their activities in face of the pandemic. This relativizes criticisms that economic damages could have prevented if the government would not have enforced a lockdown.

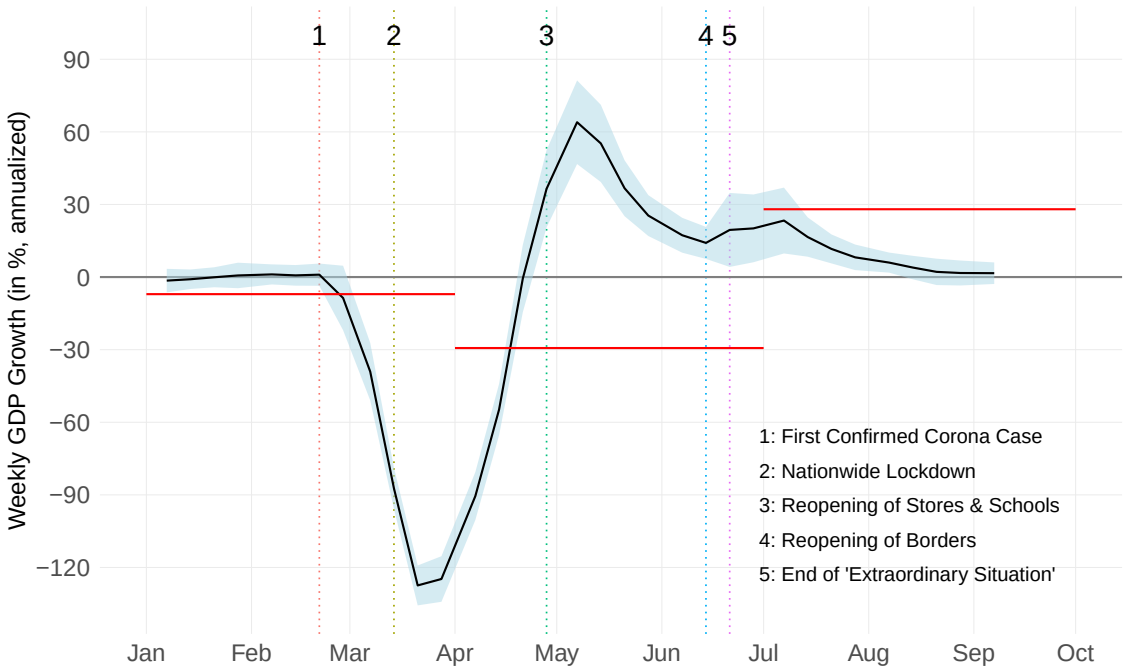

Figure 3: Weekly GDP Growth During the Corona Crisis. Notes: See Figure 1.

We have seen that the weekly GDP indicator is able to capture fluctuations of economic activity well ex-post. However, the real-time performance of the indicator might be different as it is subject to revisions caused by new information from later data publications. Figure 4 shows the indicator for its first to 30th release during the period 2005–2019.[5] Earlier releases (in yellow) tend to fluctuate more than later releases (in red and blue), especially during times of crisis. Further, the yellow lines are often lagging the red and

[5]This analysis cannot be conducted in the same way for the Corona crisis as still not enough vintages are available for the year 2020. We analyze the real-time performance of the indicator during this crisis separately in the next paragraph.

blue lines. Thus, earlier releases tend to capture macroeconomic fluctuations less quickly than would be suggested by later releases. Earlier releases rely mainly on alternative and financial high-frequency series, which are the most timely available series in the data set. Monthly series, such as business tendency surveys and retail sales, as well as realizations of quarterly GDP are included in later releases. They correct for potentially false or exaggerated signals from the alternative and financial data. For most periods, only a few revisions are necessary before the indicator closely approaches the stable state of later releases.

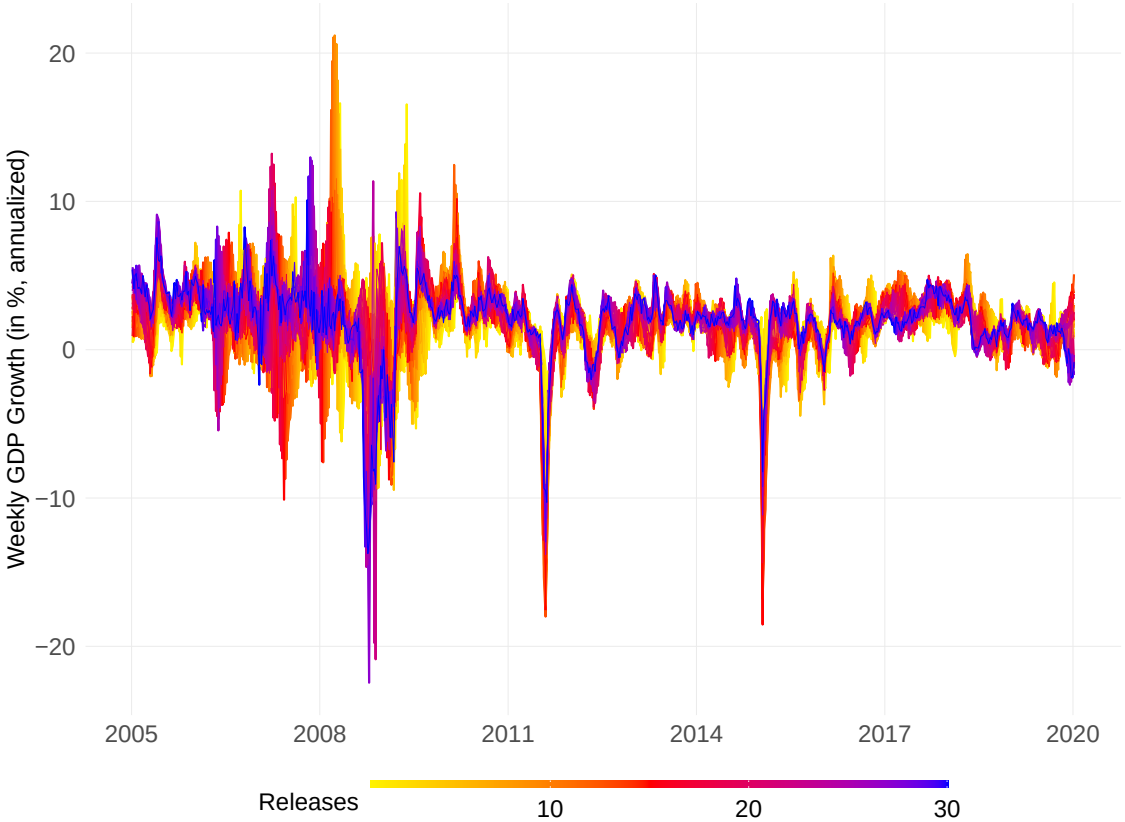

Figure 4: Revisions of the Weekly GDP Indicator. The figure compares the weekly GDP indicator for different releases in real time. The color bar goes from the first release in yellow over the 15th release in red to the 30th release in blue. The sample ranges from 2005 to 2019.

We now take a closer look on the real-time behavior of the weekly GDP indicator during the Corona crisis. Figure 5 compares the indicator as given by the last available data vintage with the real-time version of the indicator (i.e. always the first indicator release).[6] Again, the real-time version of the indicator can only rely on alternative and financial high-frequency data for its week-on-week assessment of GDP growth, as other variables are published with a delay and/or only for entire months or quarters. The figure reveals that the indicator has generally tracked the Corona crisis quite well in real time. Still,

[6]The last available data vintage for this analysis includes all data available until November 27, 2020. This will be updated in a later paper version.

the start of the strong downturn was captured in early March instead of in late February as suggested by the indicator in its last available version based on data which have been published at a later stage. Further, the real-time version of the indicator shows a slower recovery in April and May as compared to the latest vintage version of the indicator. Also, the size of both the trough in March and the rebound in May is initially underestimated. Note, however, that the annualization of the weekly GDP growth rates leads to a strong visual exaggeration of this underestimation.

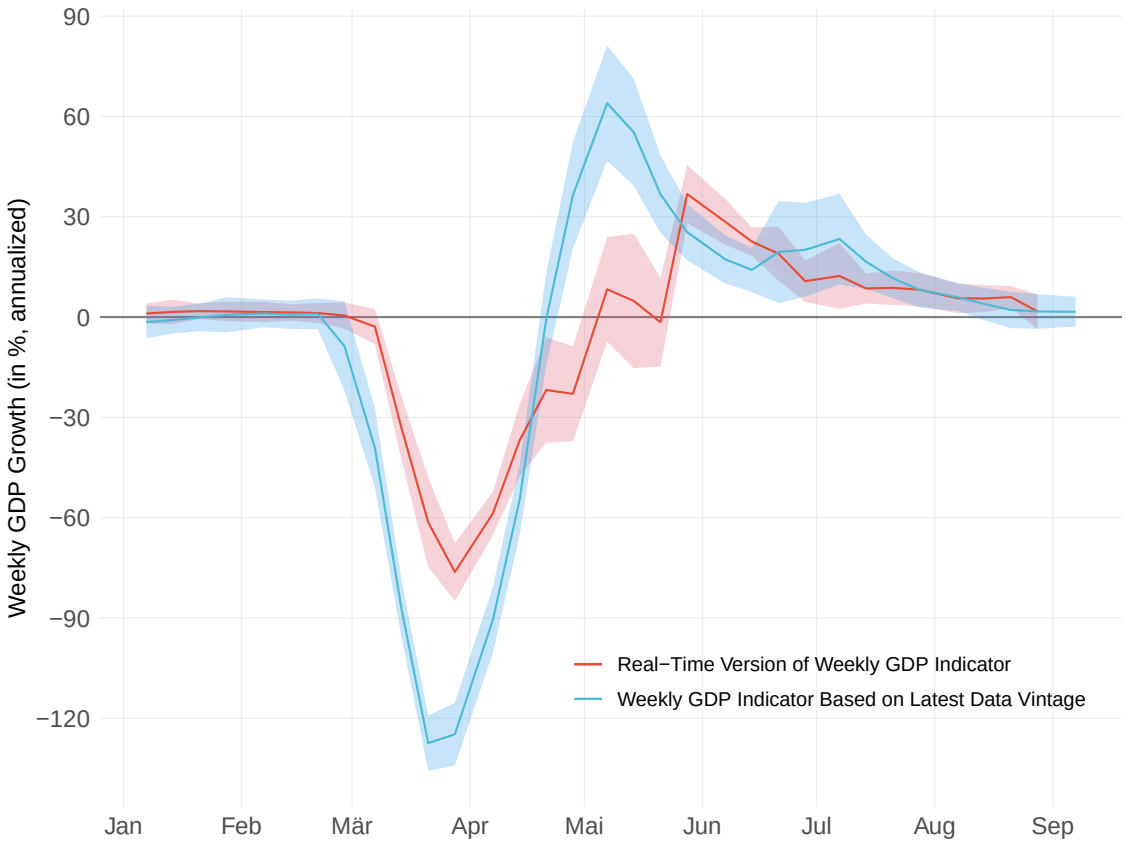

Figure 5: Real-Time Version of the Weekly GDP Indicator During the Corona Crisis. The figure compares the weekly GDP indicator as recorded by its first release ("real-time release") with the indicator as given by the last available data vintage (currently November 27, 2020). Both indicator versions are displayed with 95%-confidence intervals.

To further assess the importance of the alternative high-frequency data for capturing both the turning points as well as the extent of the Corona crisis, we compare the real-time version of the GDP indicator for three different data sets. The upper panel of Figure 6 shows the weekly GDP indicator including all data as previously (red line) in comparison with the indicator including all data, but with the alternative high-frequency data aggregated to monthly frequency (blue line).[7] The indicator using the data in weekly frequency registers the crisis much earlier. It also indicates a deeper crisis than the indicator with

[7]In order to ease comparison between the weekly updated indicator and the monthly updated indicator, both indicators are displayed by stepwise lines.

the monthly aggregated data. Further, it has smaller confidence intervals which implies that the more timely availability of the alternative data reduces the nowcast uncertainty.

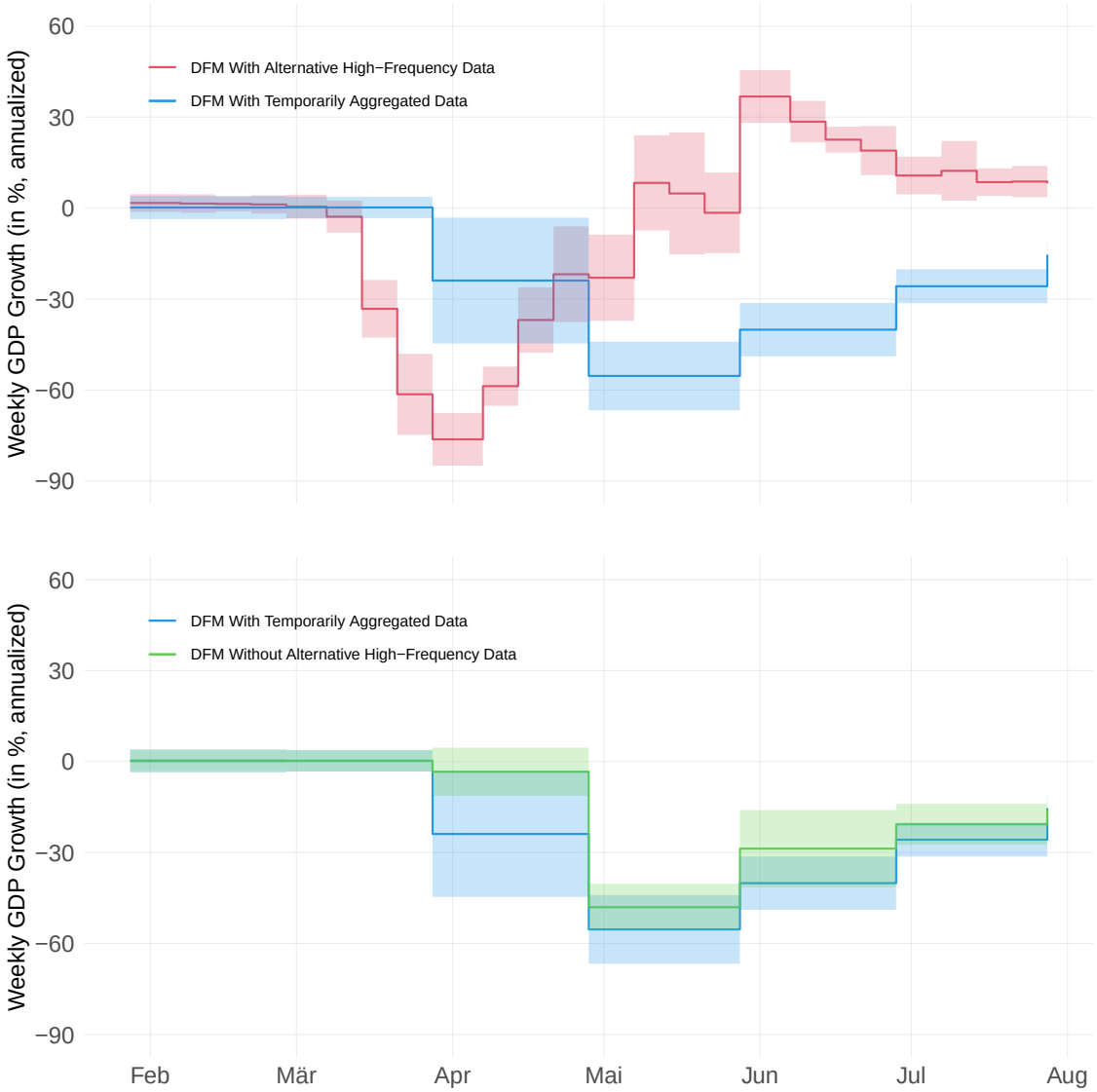

Figure 6: Real-Time Version of the GDP indicator for Different Data Sets. The figure shows the real-time version of the weekly GDP indicator based on three alternative data sets: the full data set including the alternative high-frequency data, the full data set but with the alternative high-frequency data aggregated to monthly frequency, and a data set where the alternative high-frequency data are excluded altogether. All indicator versions are displayed with 95%-confidence intervals.

The temporarily aggregated alternative data are available at the beginning of the following month together with most of the macroeconomic data in our sample. Therefore, the data are lagging the actual fluctuations of economic activity, but they might still contain valuable additional information. To inquire this, the lower panel of Figure 6 compares the indicator version including the temporarily aggregated alternative data (in blue) with a GDP indicator version where no alternative high-frequency data are included at all (in

green). While both indicator versions register the crisis at the end of March, the indicator with the temporally aggregated alternative data reacts much stronger than the indicator without the alternative data. Hence, the alternative high-frequency data contain useful information beyond their timeliness. Also, the confidence interval around the indicator with the temporally aggregated alternative data is smaller than the one around the indicator without the alternative data. This implies that the presence of the alternative data results in a decrease in nowcast uncertainty, even if they are available at a monthly frequency only. Overall, the findings suggest that the alternative high-frequency data are very helpful for capturing the economic fluctuations during the Corona crisis.

3.3 Nowcast Exercise

This section studies the usefulness of our mixed-frequency DFM by means of a pseudo real-time out-of-sample nowcast exercise for the quarter-on-quarter growth rate of real GDP. The nowcast evaluation runs from 2005Q1 to 2020Q2 and is split into crisis periods and non-crisis periods, as discussed in Section 3.1.

The nowcast performance of the mixed-frequency DFM is evaluated for different horizons. Specifically, we nowcast GDP growth of any quarter in the evaluation period from 12 weeks before its release (= "12-week nowcast horizon") up to and including the last week before its release (= "1-week nowcast horizon"). This allows us to track closely how forecast errors evolve as new data get released over time.

Figure 7 shows, for each of the 12 nowcast horizons, the root mean squared forecast errors (RMSFEs) of the DFM, using the full data set listed in Table 2, against an autoregressive (AR) model of order one with intercept.[8] The relative RMSFE for horizon h in the lower panel of the figure is defined as $ln(\text{RMSFE}^h_{\text{DFM}}) - ln(\text{RMSFE}^h_{\text{AR}})$, where $\text{RMSFE}^h_{\text{DFM}}$ ($\text{RMSFE}^h_{\text{AR}}$) is the RMSFE resulting from the DFM (AR model) nowcasts for $h = 1, \ldots, 12$.[9] Unsurprisingly, the RMSFEs of both the DFM and the AR model turn out to be substantially higher for the crisis periods than for the non-crisis periods; the strong cyclical downturns and rebounds included in the crisis periods are difficult to nowcast. The important insight is that during crisis periods, the DFM outperforms the AR model over all nowcast horizons in terms of RMSFE. The relative RMSFE improvement over the AR model increases from around 20 percent for the 12-week horizon (relative RMSFE of -0.2) to around 85 percent for the 1-week horizon (relative RMSFE of -0.85). We test for equal predictive accuracy using the test proposed by Diebold and Mariano (1995) and Giacomini and White (2006, ch. 3.4) in its one-sided version with a 10%-significance level.

[8] A simple autoregressive model has been a common benchmark in previous studies. Note that the RMSFE of the AR model does not change over the nowcast horizons, since quarterly GDP is released every 12 weeks and, hence, the first lag of GDP is available for the 12-week nowcast horizon.

[9] We show the log-difference of the two RMSFEs instead of their ratio, as the former is invariant to which of the two RMSFEs is used as the basis.

Significantly greater predictive accuracy of the forecasts stemming from the DFM is indicated by dots in the lower panels of the figure, whereas insignificance is indicated by crosses. As can be seen from the lower left panel, during crisis periods the DFM significantly outperforms the AR model in terms of predictive accuracy for most nowcast horizons. In contrast, during non-crisis periods both models perform rather equally.

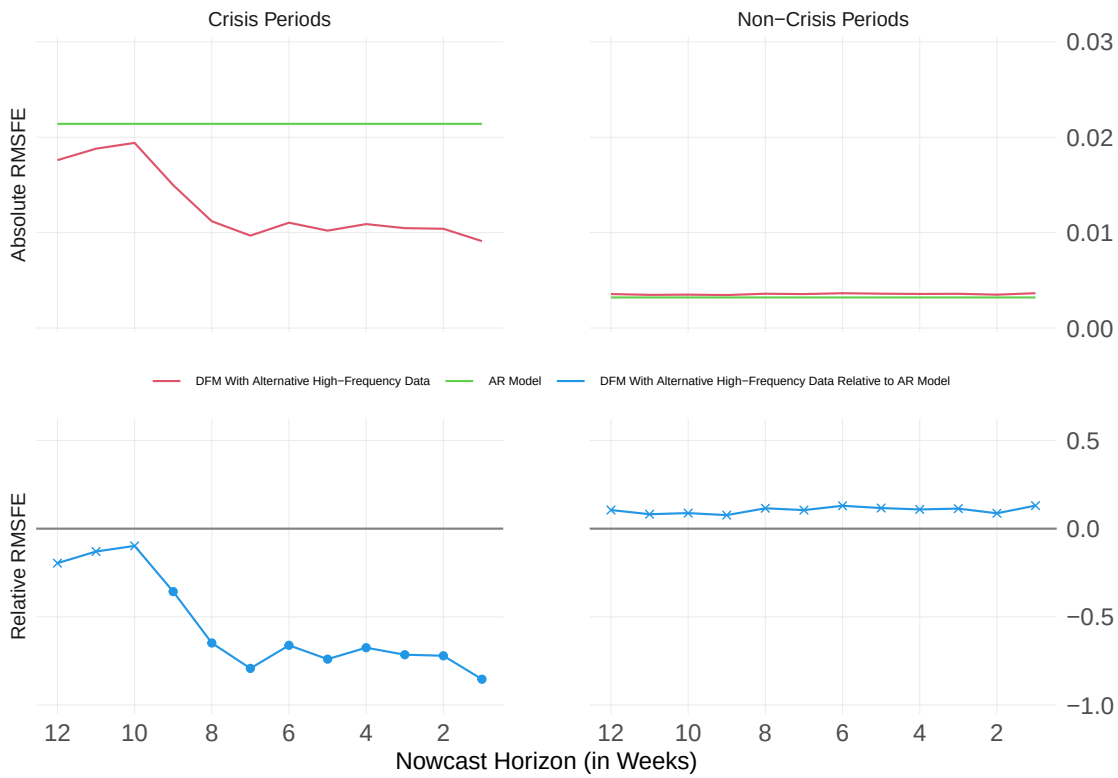

Figure 7: DFM With Alternative High-Frequency Data Against AR Model. The figure shows the RMSFEs from nowcasting quarter-on-quarter real GDP growth in a pseudo real-time out-of-sample exercise. The nowcast horizon ranges from 12 weeks before GDP release up to and including the last week before release. The evaluation spans 2005Q1–2020Q2. The crisis periods include the Great Recession, the European sovereign debt crisis, the Swiss franc shock, and the Corona crisis. The dots in the lower panels indicate differences in nowcast performance that are statistically significant at a 10%-level, according to a one-sided Diebold and Mariano (1995) test. Crosses indicate statistically insignificant differences.

A main methodological contribution of this paper is to provide a mixed-frequency DFM which can easily account for serial correlation in the errors of the factor measurement equation, despite several mixed frequencies, missing observations, ragged edges and data histories of different lengths (see Section 2.2). It turns out that this feature is indeed important for achieving a good nowcast performance in our application. This is discussed in Appendix A.8.

The DFM presented in Figure 7 uses the full data set, which includes the alternative high-frequency data as well as the standard financial and macroeconomic series. We want to know whether the use of the alternative high-frequency data, in addition to the standard

variables, actually helps to improve the nowcast performance. For this purpose, Figure 8 depicts the RMSFEs of the DFM including the full data set against the RMSFEs of the DFM, excluding the alternative high-frequency series. The DFM using the full data set clearly outperforms the DFM without the alternative high-frequency data, although only in crisis periods as can be seen from the lower left panel of the figure. Note that, for the 4- to 1-week nowcast horizons, the nowcast error difference between the two specifications is close to the chosen significance threshold with p-values being between 11 and 12 percent.

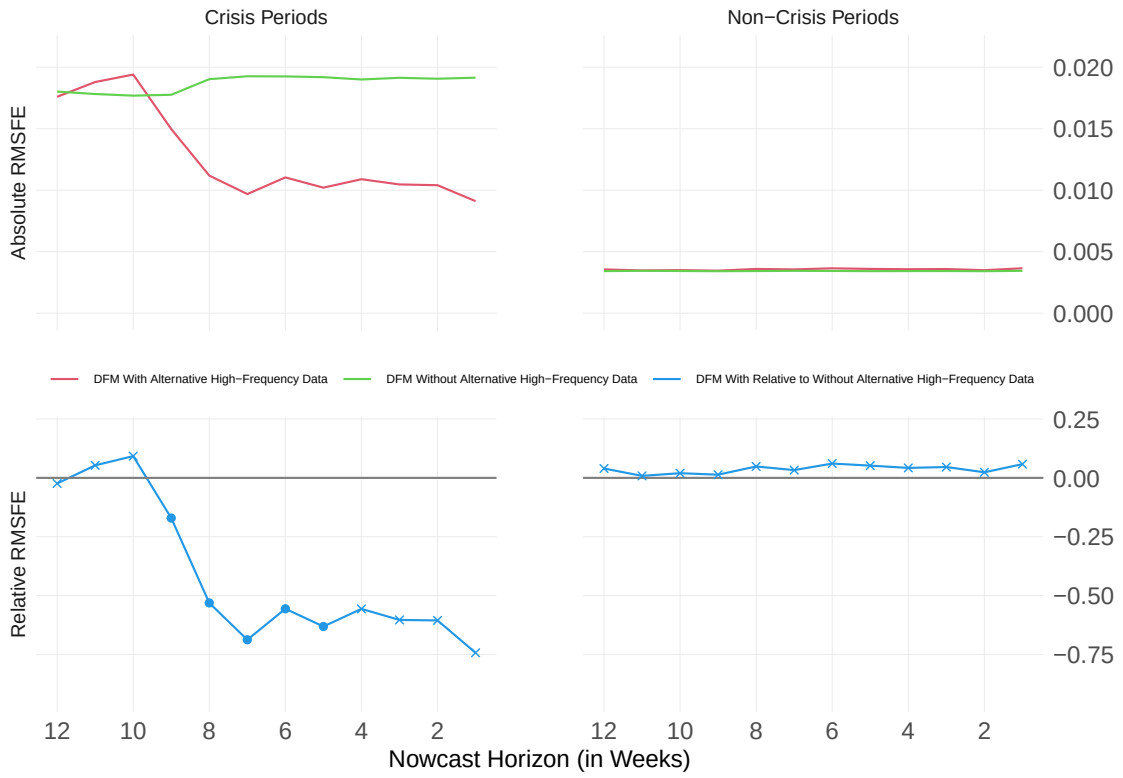

Figure 8: DFM With and Without Alternative High-Frequency Data. Notes: See Figure 7.

Further, we are interested in knowing whether the value of the alternative data for nowcasting GDP comes from its timeliness, or whether the data are even valuable if they are sampled at a monthly frequency only. Figure 9 shows the RMSFEs of the DFM including the full data set against the RMSFEs of the DFM including the full data, but with all data aggregated to the monthly frequency. These temporarily aggregated observations are available in the first week of the next month (together with, for instance, the monthly business tendency surveys). The lower left panel reveals that the higher frequency increases the nowcast performance for crisis periods. Note that, for the 5- to 1-week nowcast horizons, the difference between the two specifications is again close to the chosen significance threshold with p-values being between 11 and 13 percent.

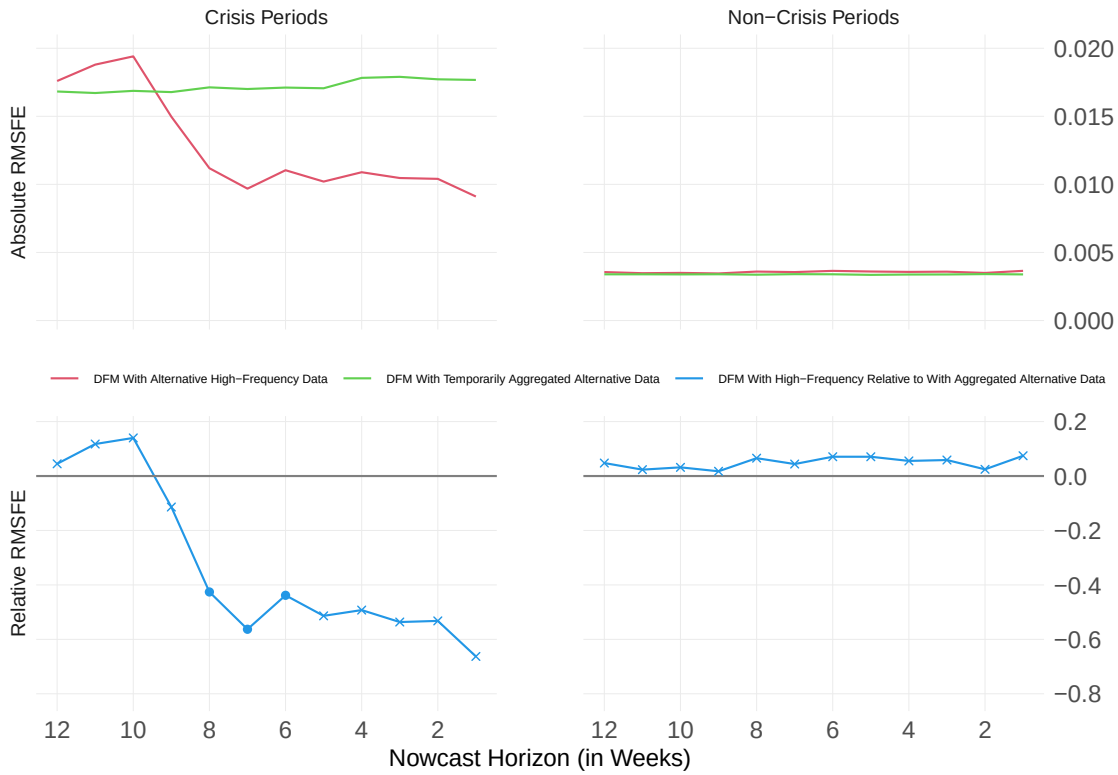

Figure 9: DFM With and Without Temporal Aggregation. Notes: See Figure 7.

In a further step, we compare the nowcast accuracy by joining the crisis and non-crisis periods to one single evaluation phase from 2005Q1 to 2020Q2. As can be seen from the blue line in the lower panel of Figure 10, the DFM including the full data set outperforms the AR model in terms of RMSFE for all horizons. The difference in the nowcast performance is statistically significant for the 9- to 7-week horizons and at least close to the chosen significance level for the 6- to 1-week horizons (p-values at 11 percent). The DFM excluding the alternative high-frequency data also outperforms the AR model (see pink line in the lower panel), although to a much smaller extent as the full data DFM. The same holds true for the DFM with the data aggregated to the monthly frequency (not shown in the figure). It is noteworthy that the differences in nowcast performance during the crisis periods almost entirely drive the RMSFE results for the joint evaluation phase, although the crisis periods account only for 12 quarters of the total 79 quarters during 2005Q1 to 2020Q2.

In order to verify the robustness of the results, Appendix A.7 presents Figures 7 to 10 with mean absolute percentage errors (MAPEs) instead of RMSFEs. The MAPE results turn out to be similar to the RMSFE results and all conclusions remain unchanged.

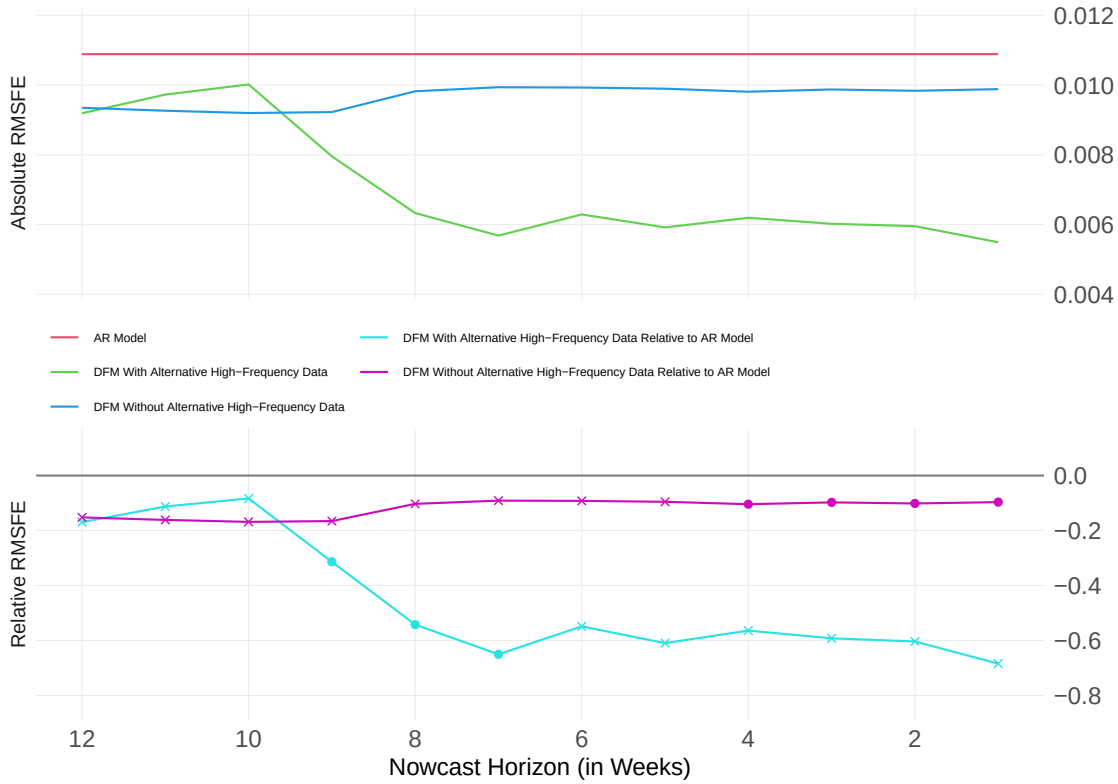

Figure 10: Joint Evaluation for Crisis and Non-Crisis Periods. Notes: See Figure 7.

4 Conclusion

In this paper, we propose a novel dynamic factor model for high- and mixed-frequency data with stochastic volatility and serial correlation in the measurement errors. The model consists of three interdependent state-space blocks: data augmentation, dynamic factor and stochastic volatility, where the former block is novel in the DFM literature. Previous mixed-frequency DFMs have disregarded unobserved information in the mixed-frequency data and have estimated a dynamic factor conditional on observed data only, typically using a modified Kalman filter. In contrast, we propose to estimate all unobserved information conditional on observed data in the data augmentation block and to estimate the dynamic factor conditional on the observed as well as the estimated latent data in the dynamic factor block. Importantly, the augmentation from sparse observed data to a balanced panel with observed and latent data information allows us to quasi-difference the measurement equation of the dynamic factor. Thereby, our DFM can easily account for serial correlation in the factor measurement errors despite mixed frequencies, publication lags, data histories of different lengths and missing observations in the data. This allows the common factor to have less explanatory power for the mixed-frequency series over a longer period of time while having high explanatory power during other periods. In contrast to previous literature, we take a fully Bayesian approach to estimate the model, where the joint posterior distribution is simulated with Gibbs sampling. A further contribution of the paper is that we extend the sampling procedure of Chan and Jeliazkov

(2009) to the case of mixed-frequency data and use it for the estimation of the latent data, the dynamic factor and the stochastic volatility. This extension is done by integrating the temporal aggregation scheme originally proposed by Mariano and Murasawa (2003) into the sampler.

As an empirical application, we construct a weekly GDP indicator using a broad set of daily, weekly, monthly and quarterly series. The set includes a variety of so-called alternative high-frequency data, such as daily credit card transactions, smartphone mobility tracking, and Google trends search queries. Our model is well suited to extract the business cycle information in these data. We look especially at four periods of sudden and strong economic fluctuations, namely the Great Recession, the European sovereign debt crisis, the Swiss franc shock and the Corona crisis. It turns that the weekly indicator tracks economic activity nicely during the aforementioned periods. The economy went down and up again so quickly during these periods that looking at monthly or quarterly figures only does not reveal the full dimension of the fluctuations. A special finding for the Corona crisis is that GDP growth fell deeply into negative territory already before the government imposed a lockdown, as consumers and producers reduced their activities in light of the pandemic. This qualifies the relevance of the lockdown for the negative economic consequences of the crisis. We take a further look at the Corona crisis and study the real-time behavior of the weekly GDP indicator during this period. Although the indicator is generally subject to revisions as more and more data become available over time, it captures the sudden and steep economic downturn and the nearly equally steep rebound during the the year 2020 quite timely and accurately in real time. We find that this is mainly due to the inclusion of the alternative high-frequency data. Our analysis further yields that even when using these data in monthly intervals only, their inclusion would still have helped to register the downturn more timely than when just using standard data. However, the main benefit comes from using the data at a high frequency.

We complement the empirical application with a pseudo real-time out-of-sample nowcast exercise for quarterly GDP from 2005Q1 to 2020Q2. It turns out that our mixed-frequency DFM significantly outperforms an AR benchmark model during crisis periods. The RMSFE decreases by between 20 and 85 percent for horizons from 12 weeks to one week before GDP release. Even when including the alternative data in monthly intervals only, they help to improve the forecast accuracy. In contrast, we find no significant improvements for non-crisis periods. We conclude that alternative high-frequency data can be very helpful when the economy moves strongly and suddenly, but they just add noise during stable times. On a last note, the differences in nowcast performance during the crisis periods turn out to be so big that they dominate the results for a joint evaluation of crisis and non-crisis periods. This is despite the fact that the crisis quarters only account for 15 percent of all quarters in the evaluation phase. The ultimate lesson here is: when constructing new nowcast models, it is of utmost importance to focus on a good perfor-

mance for major economic downturns and upturns, while normal economic times can be handled equally well with existing simple models.

References

Aruoba, S. B., Diebold, F. X., and Scotti, C. (2009). Real-Time Measurement of Business Conditions. *Journal of Business & Economic Statistics*, 27(4):417–427.

Aßmann, C., Boysen-Hogrefe, J., and Pape, M. (2016). Bayesian Analysis of Static and Dynamic Factor Models: An Ex-Post Approach Towards the Rotation Problem. *Journal of Econometrics*, 192(1):190–206.

Bai, J. and Wang, P. (2015). Identification and Bayesian Estimation of Dynamic Factor Models. *Journal of Business & Economic Statistics*, 33(2):221–240.

Bańbura, M., Giannone, D., and Reichlin, L. (2011). Nowcasting. In Clements, M. P. and Hendry, D. F., editors, *The Oxford Handbook on Economic Forecasting*, chapter 2, pages 193–224. Oxford University Press, Oxford.

Bańbura, M. and Modugno, M. (2014). Maximum Likelihood Estimation of Factor Models on Datasets with Arbitrary Pattern of Missing Data. *Journal of Applied Econometrics*, 29(1):133–160.

Camacho, M. and Perez-Quiros, G. (2010). Introducing the Euro-Sting: Short-Term Indicator of Euro Area Growth. *Journal of Applied Econometrics*, 25(4):663–694.

Carter, C. K. and Kohn, R. (1994). On Gibbs Sampling for State Space Models. *Biometrika*, 81(3):541–553.

Chan, J., Leon-Gonzalez, R., and Strachan, R. W. (2018). Invariant Inference and Efficient Computation in the Static Factor Model. *Journal of the American Statistical Association*, 113(522):819–828.

Chan, J. C. and Jeliazkov, I. (2009). Efficient Simulation and Integrated Likelihood Estimation in State Space Models. *International Journal of Mathematical Modelling and Numerical Optimisation*, 1(1-2):101–120.

Chib, S. and Greenberg, E. (1994). Bayes Inference in Regression Models With ARMA (p, q) Errors. *Journal of Econometrics*, 64(1-2):183–206.

Diebold, F. X. and Mariano, R. S. (1995). Comparing Predictive Accuracy. *Journal of Business & Economic Statistics*, 13(3):253–263.

Doz, C., Giannone, D., and Reichlin, L. (2011). A Two-Step Estimator for Large Approximate Dynamic Factor Models Based on Kalman Filtering. *Journal of Econometrics*, 164(1):188–205.

Eckert, F. and Mikosch, H. (2020). Mobility and Sales Activity During the Corona Crisis: Daily Indicators for Switzerland. *Swiss Journal of Economics and Statistics*, 156(1):1–10.

Eraslan, S. and Götz, T. (2020). An Unconventional Weekly Economic Activity Index for Germany. *Deutsche Bundesbank Technical Paper*.

Frühwirth-Schnatter, S. (1994). Data Augmentation and Dynamic Linear Models. *Journal of Time Series Analysis*, 15(2):183–202.

Giacomini, R. and White, H. (2006). Tests of Conditional Predictive Ability. *Econometrica*, 74(6):1545–1578.

Giannone, D., Reichlin, L., and Small, D. (2008). Nowcasting: The Real-Time Informational Content of Macroeconomic Data. *Journal of Monetary Economics*, 55(4):665–676.

Guggia, V., Indergand, R., and Wegmüller, P. (2020). Neuer Index zur Wöchentlichen Wirtschaftsaktivität (WWA). *Konjunkturtendenzen SECO Winter 2020/21*.

Kim, C.-J. and Nelson, C. R. (2017). *State-Space Models with Regime Switching: Classical and Gibbs-Sampling Approaches with Applications*. The MIT Press.

Kim, S., Shepherd, N., and Chib, S. (1998). Stochastic Volatility: Likelihood Inference and Comparison With ARCH Models. *Review of Economic Studies*, 65(3):361–393.

Lewis, D. J., Mertens, K., Stock, J. H., and Trivedi, M. (2020). Measuring Real Activity Using a Weekly Economic Index. *Federal Reserve Bank of New York*, 920.

Marcellino, M., Porqueddu, M., and Venditti, F. (2016). Short-Term GDP Forecasting With a Mixed-Frequency Dynamic Factor Model With Stochastic Volatility. *Journal of Business & Economic Statistics*, 34(1):118–127.

Mariano, R. S. and Murasawa, Y. (2003). A New Coincident Index of Business Cycles Based on Monthly and Quarterly Series. *Journal of Applied Econometrics*, 18(4):427–443.

Primiceri, G. E. (2005). Time Varying Structural Vector Autoregressions and Monetary Policy. *The Review of Economic Studies*, 72(3):821–852.

Stock, J. H. and Watson, M. W. (2002). Macroeconomic Forecasting Using Diffusion Indexes. *Journal of Business & Economic Statistics*, 20(2):147–162.

Tanner, M. A. and Wong, W. H. (1987). The Calculation of Posterior Distributions by Data Augmentation. *Journal of the American Statistical Association*, 82(398):528–540.

Wallis, K. F. (1986). Forecasting With an Econometric Model: The 'Ragged Edge' Problem. *Journal of Forecasting*, 5(1):1–13.

A Appendix

A.1 Temporal Aggregation

Temporal aggregation of the high frequency factor f_t to any lower frequency factor $\overline{f_t}$ is straightforward for stock variables such as interest rates or business tendency surveys. In these cases, temporal aggregation is simply given by an average:

$$\overline{f_t} = \sum_{i=0}^{k-1} \lambda_i \; f_{t-i}, \quad \text{where} \quad \lambda_i = \tfrac{1}{k}$$

and where k denotes how many times the high frequency occurs within the low frequency (e.g., $k = 3$ for aggregation of monthly to quarterly data). The case of flow variables, such as GDP or retail sales, is slightly more complicated. Since these variables typically enter forecasting models in growth rates, any temporal aggregation involves nonlinearities. An approximation based on geometric instead of arithmetic means has been proposed by Mariano and Murasawa (2003) and has since been widely adopted (see, e.g., Bańbura et al., 2011, and Marcellino et al., 2016):

$$\overline{f_t} = \sum_{i=0}^{s} \lambda_i \; f_{t-i}, \quad \text{where} \quad \lambda_i = \tfrac{k-|1+i-k|}{k}$$

and where the number of distributed lags is given by $s = 2(k-1)$. The geometric mean based aggregation implies a triangular weighting scheme that accounts for the statistical overhang occuring during the aggregation of growth rates. This is illustrated in the following: Let X be a flow variable and let

$$\log X_{Q1} = \frac{1}{3}(\log X_{Jan} + \log X_{Feb} + \log X_{Mar}).$$

Growth in the second quarter is then given by

$$\begin{aligned}
&\log X_{Q2} - \log X_{Q1} = \\
&\quad \frac{1}{3}(\log(X_{Jun} + \log X_{May} + \log X_{Apr}) - \frac{1}{3}(\log X_{Mar} + \log X_{Feb} + \log X_{Jan}) \\
&= \frac{1}{3}(\log X_{Jun} - \log X_{Mar}) + \frac{1}{3}(\log X_{May} - \log X_{Feb}) + \frac{1}{3}(\log X_{Apr} - \log X_{Jan}).
\end{aligned}$$

Next, introduce additional terms into the equation:

$$\begin{aligned}
&\log X_{Q2} - \log X_{Q1} = \\
&\quad \frac{1}{3}(\log X_{Jun} - \log X_{May} + \log X_{May} - \log X_{Apr} + \log X_{April} - \log X_{Mar}) + \\
&\quad \frac{1}{3}(\log X_{May} - \log X_{Apr} + \log X_{Apr} - \log X_{Mar} + \log X_{Mar} - \log X_{Feb}) + \\
&\quad \frac{1}{3}(\log X_{Apr} - \log X_{Mar} + \log X_{Mar} - \log X_{Feb} + \log X_{Feb} - \log X_{Jan}).
\end{aligned}$$

Defining growth rates as $x_t = \log X_t - \log X_{t-1}$, the previous equation simplifies to

$$\begin{aligned} x_{Q2} =& \frac{1}{3}(x_{Jun} + x_{May} + x_{April}) + \frac{1}{3}(x_{May} + x_{April} + x_{March}) \\ &+ \frac{1}{3}(x_{April} + x_{March} + x_{Feb}) \\ =& \frac{1}{3}x_{Jun} + \frac{2}{3}x_{May} + \frac{3}{3}x_{April} + \frac{2}{3}x_{March} + \frac{1}{3}x_{Feb}. \end{aligned}$$

This triangular weighting structure enters the distributed lag matrices $\mathbf{L}_0, \ldots, \mathbf{L}_s$ in Equation (2). It furthermore highlights the fact that high-frequency growth rates affect low frequency growth in the next period, a phenomenon that is commonly referred to as statistical overhang or carry-over effect.

A.2 Mixture Distribution

The error term in the measurement equation for the stochastic volatility factor follows a $\log \chi^2(1)$-distribution (see Equation (8)). In order for the state space model to be of linear Gaussian form, we approximate the moments of the distribution by a mixture of normals as described in Kim et al. (1998) (see also Primiceri, 2005). A mixture of seven normal distributions is used, where distribution $j = 1, \ldots, 7$ has mean μ_j and variance ξ_j and is selected with probability q_j. The parameters and the selection probabilites are chosen exactly as in Kim et al. (1998) and are shown in Table 1.

Table 1. Parameters and Selection Probabilities of Mixing Distribution

j	q_j	μ_j	ξ_j
1	0.00730	-11.40039	5.79596
2	0.10556	-5.24321	2.61369
3	0.00002	-9.83726	5.17950
4	0.04395	1.50746	0.16735
5	0.34001	-0.65098	0.64009
6	0.24566	0.52478	0.34023
7	0.25750	-2.35859	1.26261

Note that $\mu_j + 1.2704$ equals m_i from Table 4 of Kim et al. (1998), with the constant term being present in Equations (9) and (10).

A.3 Stochastic Volatility Estimation

For notational convenience, let $w_t = \log\Big((f_t - \phi_1 f_{t-1} + \ldots + \phi_p f_{t-p})^2 + c\Big)$.[10] In order to estimate the stochastic volatility factor h_t, the measurement equation for h_t given in Equation (8) is stacked over all periods $t = 1, \ldots, T$ to get

$$\mathbf{w} = \mathbf{W}\mathbf{h} - \boldsymbol{\mu} + \boldsymbol{\varepsilon}, \qquad \boldsymbol{\varepsilon} \sim \mathcal{N}(\mathbf{0}, \boldsymbol{\Xi})$$

[10] Note that no values exist for $w_{1-s}, \ldots, w_{1-s+p-1}$ since f_{1-s} is the first estimated factor (see Equation (12)). We simply assume that these w_t-values are zero.

where

$$\underset{(T+s)\times 1}{\mathbf{w}} = \begin{bmatrix} w_{1-s} \\ \vdots \\ w_1 \\ \vdots \\ w_T \end{bmatrix}, \qquad \underset{(T+s)\times(T+s)}{\mathbf{W}} = \begin{bmatrix} 2 & & & & \\ & 2 & & & \\ & & \ddots & & \\ & & & 2 & \\ & & & & 2 \end{bmatrix}, \qquad \underset{(T+s)\times 1}{\mathbf{h}} = \begin{bmatrix} h_{1-s} \\ \vdots \\ h_1 \\ \vdots \\ h_T \end{bmatrix}$$

Each element of vector $\boldsymbol{\mu}$ is filled with a specific $\mu_j \in [\mu_1, \ldots, \mu_7]$ from Table 1 with j having been selected according to the probablities displayed in the table. Each element of the diagonal matrix $\boldsymbol{\Xi}$ contains the corresponding $\xi_j \in [\xi_1, \ldots, \xi_7]$ from the table.

We have no prior knowledge about the initial state of the stochastic volatility. Thus, we follow Chan and Jeliazkov (2009) in imposing a diffuse prior by stacking the stochastic volatility state equation from Equation (7) such that

$$\mathbf{N}\mathbf{h} = \mathbf{u}, \qquad \mathbf{u} \sim \mathcal{N}(\mathbf{0}, \omega \mathbf{I}_{T+s})$$

where $\mathbf{N}$ is of reduced rank and is given by

$$\underset{(T+s-1)\times(T+s)}{\mathbf{N}} = \begin{bmatrix} -1 & 1 & & \\ & \ddots & \ddots & \\ & & -1 & 1 \end{bmatrix}.$$

The precision matrix $\mathbf{Q}_0$ is then given by $\mathbf{N}'(\omega \mathbf{I}_{T+s})^{-1}\mathbf{N}$ and the conditional posterior of the stochastic volatility is normally distributed according to

$$\mathbf{h} \sim \mathcal{N}(\mathbf{q}_1, \mathbf{Q}_1) \quad \text{where} \quad \begin{aligned} \mathbf{Q}_1 &= \left(\mathbf{Q}_0 + \mathbf{W}'\boldsymbol{\Xi}^{-1}\mathbf{W}\right)^{-1} \\ \mathbf{q}_1 &= \mathbf{Q}_1 \left(\mathbf{W}'\boldsymbol{\Xi}^{-1}(\mathbf{w} + \boldsymbol{\mu})\right). \end{aligned}$$

As is the case for the dynamic factor, this algorithm is computationally very efficient if block-banded matrix algorithms are used and sparse matrices are preallocated.

A.4 Latent Data Estimation

In order to group the parameters in appropriate blocks, the measurement equation for $\mathbf{x}_t$ given in Equation (9) is stacked over all time periods $t = 1, \ldots, T$. This gives

$$\mathbf{y} = \mathbf{S}\mathbf{x} + \boldsymbol{\epsilon}, \qquad \boldsymbol{\epsilon} \sim \mathcal{N}(\mathbf{0}, \mathbf{I}_T \otimes \epsilon \mathbf{I}_n)$$

where $\mathbf{y} = [\mathbf{y}_1', \ldots, \mathbf{y}_T']'$, $\mathbf{x} = [\mathbf{x}_1', \ldots, \mathbf{x}_T']'$ and $\mathbf{S} = \text{diag}(\mathbf{S}_1, \ldots, \mathbf{S}_T)$. The state equation for $\mathbf{x}_t$ shown in Equation (10) is stacked correspondingly:

$$\mathbf{K}\mathbf{x} = \mathbf{G}\mathbf{f} + \mathbf{u}, \qquad \mathbf{u} \sim \mathcal{N}(\mathbf{0}, \mathbf{I}_T \otimes \boldsymbol{\Sigma}) \tag{13}$$

where $\mathbf{G}$ has been defined in Equation (11) and

$$\underset{nT\times nT}{\mathbf{K}} = \begin{bmatrix} \mathbf{I}_n & & & \\ -\boldsymbol{\rho} & \mathbf{I}_n & & \\ & \ddots & \ddots & \\ & & -\boldsymbol{\rho} & \mathbf{I}_n \end{bmatrix}.$$

The precision matrix $\mathbf{P}_0$ is then given by $\mathbf{K}'(\mathbf{I}_T \otimes \boldsymbol{\Sigma})^{-1}\mathbf{K}$ and the conditional posterior of $\mathbf{x}$ follows a normal distribution according to

$$\begin{aligned} \mathbf{x} \sim \mathcal{N}(\mathbf{p}_1, \mathbf{P}_1) \quad \text{where} \quad \mathbf{P}_1 &= \left(\mathbf{P}_0 + \mathbf{S}'(\mathbf{I}_T \otimes \epsilon\mathbf{I}_n)^{-1})\mathbf{S}\right)^{-1} \\ \mathbf{p}_1 &= \mathbf{P}_1 \left(\mathbf{K}_{-1}' \left(\mathbf{I}_{T-1} \otimes \boldsymbol{\Sigma}\right)^{-1} \mathbf{G}\mathbf{f} + \mathbf{S}'(\mathbf{I}_T \otimes \epsilon\mathbf{I}_n)^{-1})\mathbf{y}\right) \end{aligned}$$

with $\mathbf{K}_{-1}$ being $\mathbf{K}$ without the first n rows. The conditional posterior of $\mathbf{x}$ is, therefore, essentially a weighted average of $\mathbf{y}$ and of a projection using $\mathbf{G}\mathbf{f}$. The variable-specific weights derive from $\mathbf{S}$ and take values zero or one. Specifically, when a variable is observed and, hence, the corresponding entry in $\mathbf{y}_t$ is non-zero, its weight is one and the respective entry in $\mathbf{x}_t$ is (approximately) equal to this actual observation. In contrast, when a variable is not observed and the corresponding entry in $\mathbf{y}_t$ is zero, its weight is zero and the corresponding entry in $\mathbf{x}_t$ is equal to the projection estimate.

A.5 Estimation of Remaining Parameters

Factor Loadings. To estimate the factor loadings $\boldsymbol{\lambda}$, we stack the quasi-differenced measurement equation of Equation (5) over all time periods $t = 1, \ldots, T$. This gives

$$\tilde{\mathbf{x}} = \mathbf{Z}\boldsymbol{\lambda} + \mathbf{u}, \quad \mathbf{u} \sim \mathcal{N}\left(\mathbf{0}, \mathbf{I}_T \otimes \boldsymbol{\Sigma}\right)$$

where

$$\underset{n(T-1)\times n}{\mathbf{Z}} = \sum_{i=0}^{s} \begin{bmatrix} f_{2-i}\mathbf{D}_i \\ \vdots \\ f_{T-i}\mathbf{D}_i \end{bmatrix}, \quad \mathbf{D}_i = \begin{cases} \mathbf{L}_0, & \text{if } i = 0. \\ -\boldsymbol{\rho}\mathbf{L}_s, & \text{if } i = s. \\ \mathbf{L}_{i-1} - \boldsymbol{\rho}\mathbf{L}_i, & \text{otherwise.} \end{cases}$$

The conditional posterior distribution of the factor loadings is then given by

$$\boldsymbol{\lambda} \sim \mathcal{N}\left(\mathbf{b}_1, \mathbf{B}_1\right) \quad \text{where} \quad \mathbf{B}_1 = \left(\mathbf{B}_0^{-1} + \mathbf{Z}'(\mathbf{I}_{T-1} \otimes \boldsymbol{\Sigma}^{-1})\mathbf{Z}\right)^{-1}$$
$$\mathbf{b}_1 = \mathbf{B}_1 \left(\mathbf{B}_0^{-1}\mathbf{b}_0 + \mathbf{Z}'(\mathbf{I}_{T-1} \otimes \boldsymbol{\Sigma}^{-1})\tilde{\mathbf{x}}\right).$$

The prior mean vector $\mathbf{b}_0$ is chosen to be a vector of ones. To identify the dynamic factor, in line with Bai and Wang (2015), the prior variance of the factor loading on GDP, λ_{gdp}, is set to 10^{-9}. This shrinks λ_{gdp} strongly towards one and is sufficient to identify the model. Furthermore, setting λ_{gdp} to one and ρ_{gdp} to zero ensures that the dynamic factor is, in expectation, equal to the standardized weekly quarter-on-quarter (i.e. the 12-weeks-on-12-weeks) growth rate of GDP, provided that it is temporally aggregated according to Mariano and Murasawa (2003). Setting the remaining prior variances in $\mathbf{B}_0$ to very large values leads to uninformative priors for the other factor loadings.

Error Covariance in Factor Measurement Equation. In order to estimate the covariance matrix $\boldsymbol{\Sigma}$ of the serially uncorrelated measurement errors in the quasi-differenced measurement equation given in Equation (5), simply retrieve the stacked measurement errors from $\tilde{\mathbf{x}} - \mathbf{Z}\boldsymbol{\lambda}$. We assume $\boldsymbol{\Sigma}$ to be diagonal, which reflects our belief that the dynamic factor accounts for a majority of the cross-correlation in the data. As a consequence, the error variances σ_i^2 can be drawn equation-by-equation from an inverse Gamma distribution:

$$\sigma_i^2 \sim \mathcal{IG}\left(c_{1,i}/2, d_{1,i}/2\right) \quad \text{where} \quad c_{1,i} = c_{0,i} + T$$
$$d_{1,i} = d_{0,i} + \mathbf{u}_i\mathbf{u}_i'.$$

With the exception of the measurement error variance on GDP growth, the priors are selected uninformative by setting $c_{0,i} = 3$ and $d_{0,i} = 1$. For σ_{gdp}^2, we select an informative prior with $c_{0,\text{gdp}} = 10^{-9}$ and $d_{0,\text{gdp}} = 0.05 \times 10^{-9}$. Since we identify the dynamic factor as the high-frequency growth rate of GDP, this determines how closely the temporally aggregated factor tracks the observed values. There are, of course, many prior choices feasible, even completely uninformative ones. These particular parameters fix the measurement error for GDP growth at a specific value, which allows us to determines exactly by how much the dynamic factor is allowed to deviate from the actual observations.

Autoregressive Coefficients of Factor Measurement Errors. The autoregressive coefficients in matrix $\boldsymbol{\rho}$ of Equation (3) are estimated from the serially correlated measurement errors of Equation (2). These measurement errors are collected from $\mathbf{x}_t - \mathbf{L}_0\boldsymbol{\lambda}f_t + \mathbf{L}_1\boldsymbol{\lambda}f_{t-1} + \ldots + \mathbf{L}_s\boldsymbol{\lambda}f_{t-s}$ for $t = 1, \ldots, T$. We draw the diagonal elements of $\boldsymbol{\rho}$ equation-by-equation, using the vector $\mathbf{e}_i$ which contains the serially correlated errors from the ith variable. The conditional posterior distribution of the diagonal elements $\rho_i, \ldots, \rho_n$ is then

given by

$$\rho_i \sim \mathcal{N}\left(r_{1,i}, R_{1,i}\right) \quad \text{where} \quad R_{1,i} = \left(R_{0,i}^{-1} + \sigma_i^{-2}\mathbf{e}_{i,-T}'\mathbf{e}_{i,-T}\right)^{-1}$$
$$r_{1,i} = R_{1,i}\left(R_{0,i}^{-1}r_{0,i} + \sigma_i^{-2}\mathbf{e}_{i,-T}'\mathbf{e}_{i,-1}\right).$$

We set the prior mean $r_{0,i} = 0$ for all variables i. Since we want the dynamic factor to track GDP growth closely and without any serial correlation in the errors, we set the prior variance $R_{0,\text{gdp}} = 10^{-9}$. This shrinks ρ_{gdp} towards zero. For the remaining parameters, we set $R_{0,i} = 1$, which is rather uninformative.

Autoregressive Coefficients of Factor State Equation. The autoregressive coefficients $\phi_1, \ldots, \phi_p$ are obtained following Chan et al. (2018). The state equation for the factor given in Equation (6) is stacked over all periods $t = p+1, \ldots, T$ to get

$$\mathbf{m} = \mathbf{M}\boldsymbol{\phi} + \mathbf{v}, \quad \mathbf{v} \sim \mathcal{N}\left(\mathbf{0}, \mathbf{V}\right)$$

where

$$\mathbf{m} = \begin{bmatrix} f_{p+1} \\ \vdots \\ f_T \end{bmatrix}, \quad \mathbf{M} = \begin{bmatrix} f_p & \cdots & f_1 \\ \vdots & \ddots & \vdots \\ f_{T-1} & \cdots & f_{T-p} \end{bmatrix}, \quad \boldsymbol{\phi} = \begin{bmatrix} \phi_1 \\ \vdots \\ \phi_p \end{bmatrix}$$

and where $\mathbf{V}$ is a diagonal matrix containing the time-varying variances of the state equation $e^{2h_{p+1}}, \ldots, e^{2h_T}$. The conditional posterior is given by

$$\boldsymbol{\phi} \sim \mathcal{N}\left(\mathbf{a}_1, \mathbf{A}_1\right) \quad \text{where} \quad \mathbf{A}_1 = \left(\mathbf{A}_0^{-1} + \mathbf{M}'\mathbf{V}^{-1}\mathbf{M}\right)^{-1}$$
$$\mathbf{a}_1 = \mathbf{A}_1\left(\mathbf{A}_0^{-1}\mathbf{a}_0 + \mathbf{M}'\mathbf{V}^{-1}\mathbf{m}\right).$$

The priors are chosen to be uninformative with mean zero and prior variance one. There is no need for shrinkage since we use $p = 1$ in our empirical application. Increasing the lag length might require additional shrinkage priors to control the parameter space. For data sets with limited availablity of historical data or poor data quality it might be useful to enforce stationarity of the process. This can be done by discarding draws where the largest absolute eigenvalue of the companion matrix is larger than a certain threshold, typically 1. We have found robust convergence by setting this threshold to 3/4 and, therefore, encouraging a certain degree of stationarity.

Error Variance in Stochastic Volatility State Equation. The variance ω of the errors in the state equation of the stochastic volatility factor displayed in Equation (7) is

drawn from an inverse gamma distribution according to

$$\omega \sim \mathcal{IG}\left(k_1/2, l_1/2\right) \quad \text{where} \quad \begin{aligned} k_1 &= k_0 + T + s \\ l_1 &= l_0 + \mathbf{v}\mathbf{v}'. \end{aligned}$$

$\mathbf{v}$ contains the residuals from the stochastic volatility state equation. We use uninformative priors with $k_0 = 3$ and $l_0 = 1$.

A.6 Data Overview

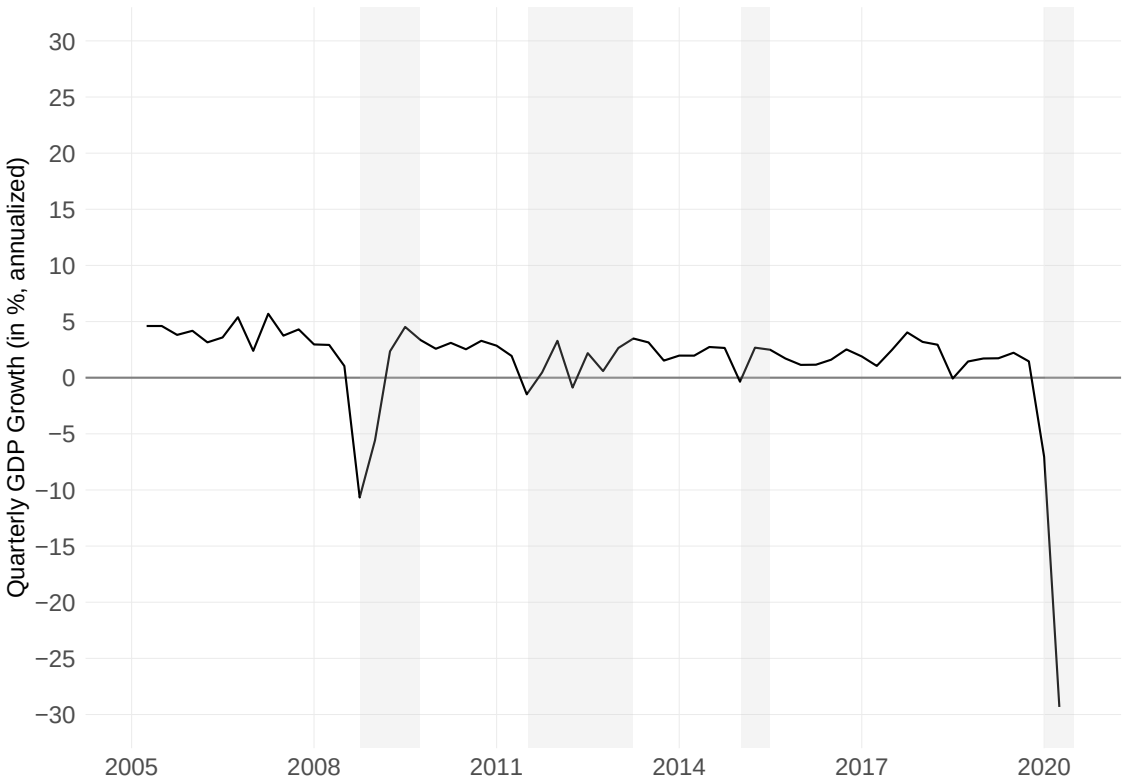

Figure 11: History of Swiss GDP Growth. The figure shows the annualized quarter-on-quarter growth rate of Swiss real GDP, adjusted for financial inflows and outflows stemming from international sport events, in percent from 2005Q1 to 2020Q2. The crisis periods are indicated by vertical grey bars.

Table 2. Data Overview

Name	Category	Frequency	Release Lag	Start Date	Unit	Transformation	Type	Source
Google Search Index, Perceived Economic Situation	Alternative	Daily	1W	2006W1	Index	None	Stock	Trendecon
Google Search Index, Perceived Labour Market Situation	Alternative	Daily	1W	2006W1	Index	None	Stock	KOF
Passenger Car Frequency, Counting Stations on Major Swiss Motorways	Alternative	Daily	1W	2006W2	Actual	Log Difference	Flow	ASTRA
Truck Frequency, Counting Stations on Major Swiss Motorways	Alternative	Daily	1W	2006W2	Actual	Log Difference	Flow	ASTRA
Truck-Toll Mileage Index, Germany	Alternative	Daily	1W	2008W2	Actual	Log Difference	Flow	Destatis
Energy Consumed by Swiss End Users	Alternative	Daily	1W	2009W2	kWh	Log Difference	Flow	Swissgrid
Energy Production in Switzerland	Alternative	Daily	1W	2009W2	kWh	Log Difference	Flow	Swissgrid
Total Flight Arrivals, Zurich Airport	Alternative	Daily	1W	2011W2	Actual	Log Difference	Flow	Zurich Airport
Total Flight Departures, Zurich Airport	Alternative	Daily	1W	2011W2	Actual	Log Difference	Flow	Zurich Airport
Cash Withdrawals, Swiss-Wide Volume in CHF	Alternative	Daily	1W	2018W2	CHF, in Millions	Log Difference	Flow	SIX Group
Non-Online Retail Sales, Swiss-Wide Volume in CHF	Alternative	Daily	1W	2018W2	CHF, in Millions	Log Difference	Flow	SIX Group
Swiss Debit Card Transactions Abroad, Volume in CHF	Alternative	Daily	1W	2018W2	CHF, in Millions	Log Difference	Flow	SIX Group
Credit Card Transactions, Swiss-Wide Frequency	Alternative	Weekly	1W	2020W2	Actual, in Thousands	Log Difference	Flow	SPA
Median Day Distance of Representative Swiss Population Sample	Alternative	Daily	1W	2020W2	km	Log Difference	Flow	intervista
Private Transport Frequency, Important Counting Stations, Zurich	Alternative	Daily	1W	2020W2	Actual	Log Difference	Flow	StatistikZH
Public Transport Passenger Frequency, Zurich Main Station	Alternative	Daily	1W	2020W2	Actual	Log Difference	Flow	SBB
Google COVID-19 Community Mobility Reports, Grocery and Pharmacy	Alternative	Daily	1W	2020W7	Percentage	Log Difference	Flow	Google
Google COVID-19 Community Mobility Reports, Parks	Alternative	Daily	1W	2020W7	Percentage	Log Difference	Flow	Google
Google COVID-19 Community Mobility Reports, Residential	Alternative	Daily	1W	2020W7	Percentage	Log Difference	Flow	Google
Google COVID-19 Community Mobility Reports, Retail and Recreation	Alternative	Daily	1W	2020W7	Percentage	Log Difference	Flow	Google
Google COVID-19 Community Mobility Reports, Transit Stations	Alternative	Daily	1W	2020W7	Percentage	Log Difference	Flow	Google
Google COVID-19 Community Mobility Reports, Workplaces	Alternative	Daily	1W	2020W7	Percentage	Log Difference	Flow	Google
Public Transport Passenger Frequency, Zurich Hardbruecke	Alternative	Daily	1W	2020W15	Actual	Log Difference	Flow	SBB
10-Year Confederation Bond Yield	Financial	Monthly	5W	1990M1	Percentage	Detrended	Stock	SECO
Swiss Market Index (SMI)	Financial	Daily	1W	1990W1	CHF	Log Difference	Flow	SIX Group
Swiss Stock Market Index, Consumer Discretionary	Financial	Daily	1W	1990W1	CHF	Log Difference	Flow	Datastream
Swiss Stock Market Index, Consumer Staples	Financial	Daily	1W	1990W1	CHF	Log Difference	Flow	Datastream
Swiss Stock Market Index, Financials	Financial	Daily	1W	1990W1	CHF	Log Difference	Flow	Datastream
Swiss Stock Market Index, Industrials	Financial	Daily	1W	1990W1	CHF	Log Difference	Flow	Datastream
3-Month CHF LIBOR	Financial	Monthly	5W	1991M12	Percentage	Detrended	Stock	SNB
Consumer Price Index, Total	Prices	Monthly	5W	1990M1	Index, 2015M12=100	Log Difference	Flow	SECO
Producer Prices Index	Prices	Monthly	5W	1990M1	Index, 2015M12=100	Log Difference	Flow	SECO
Consumer Price Index, Excl. Energy, Fresh & Seasonal Products	Prices	Monthly	5W	2000M6	Index, 2015M12=100	Log Difference	Flow	SECO
Gross Domestic Product, Adjusted for International Sport Events	Production	Quarterly	9W	1990Q1	CHF, Real Prices	Log Difference	Flow	SECO
Retail Sales, Culture and Recreation Goods, Constant Prices	Retail	Monthly	9W	2000M2	Index, 2015=100	Log Difference	Flow	SECO
Retail Sales, Food, Beverage and Tobacco	Retail	Monthly	9W	2000M2	Index, 2015=100	Log Difference	Flow	SECO
Retail Sales, Household Equipment	Retail	Monthly	9W	2000M2	Index, 2015=100	Log Difference	Flow	SECO
Retail Sales, Information and Communication Equipment	Retail	Monthly	9W	2000M2	Index, 2015=100	Log Difference	Flow	SECO
Retail Sales, Non-Food	Retail	Monthly	9W	2000M2	Index, 2015=100	Log Difference	Flow	SECO
Retail Sales, Other Goods	Retail	Monthly	9W	2000M2	Index, 2015=100	Log Difference	Flow	SECO
Retail Sales, Total	Retail	Monthly	9W	2000M2	Index, 2015=100	Log Difference	Flow	SECO
Purchasing Managers Index, Manufacturing Sector	Survey	Monthly	5W	1995M1	Index (Diffusion)	None	Stock	Credit Suisse
Purchasing Managers Index, Manufacturing Sector, Backlog of Orders	Survey	Monthly	5W	1995M1	Index (Diffusion)	None	Stock	Credit Suisse
Purchasing Managers Index, Manufacturing Sector, Output	Survey	Monthly	5W	1995M1	Index (Diffusion)	None	Stock	Credit Suisse
Business Situation Assessment, Manufacturing	Survey	Monthly	5W	2004M2	Net Balance	Log Difference	Flow	KOF
Business Situation Assessment, Manufacturing Consumption Goods	Survey	Monthly	5W	2004M2	Net Balance	Log Difference	Flow	KOF
Business Situation Assessment, Manufacturing Durable Goods	Survey	Monthly	5W	2004M2	Net Balance	Log Difference	Flow	KOF
Business Situation Assessment, Manufacturing Intermediate Goods,	Survey	Monthly	5W	2004M2	Net Balance	Log Difference	Flow	KOF
Business Situation Assessment, Manufacturing Investment Goods	Survey	Monthly	5W	2004M2	Net Balance	Log Difference	Flow	KOF
Business Situation Assessment, All Industries	Survey	Monthly	5W	2009M5	Net Balance	Log Difference	Flow	KOF
Business Situation Assessment, Finance & Insurance	Survey	Monthly	5W	2010M8	Net Balance	Log Difference	Flow	KOF
Business Situation Assessment, Construction	Survey	Monthly	5W	2011M5	Net Balance	Log Difference	Flow	KOF
Business Situation Assessment, Project Engineering	Survey	Monthly	5W	2011M5	Net Balance	Log Difference	Flow	KOF

***Notes*: "W" stands for week, "M" for month, and "Q" for quarter. All series refer to Switzerland, if not indicated otherwise. In particular, the Google search indices comprises searches in Switzerland. All monthly series are seasonally adjusted. The release lag for each variable is chosen based on the releases in the year 2020. Detrending of a variable (see column "Transformation") is done by substracting the rolling in-sample moving average of three times the frequency of the respective variable. *Abbreviations of sources*: ASTRA: Swiss Federal Roads Office, Destatis: German Federal Statistical Office, KOF: Swiss Economic Institute, SECO: Swiss State Secretariat for Economic Affairs, SPA: Swiss Payment Association, StatistikZH: Statistical Office of the Canton of Zurich.**

A.7 Mean Absolute Percentage Errors

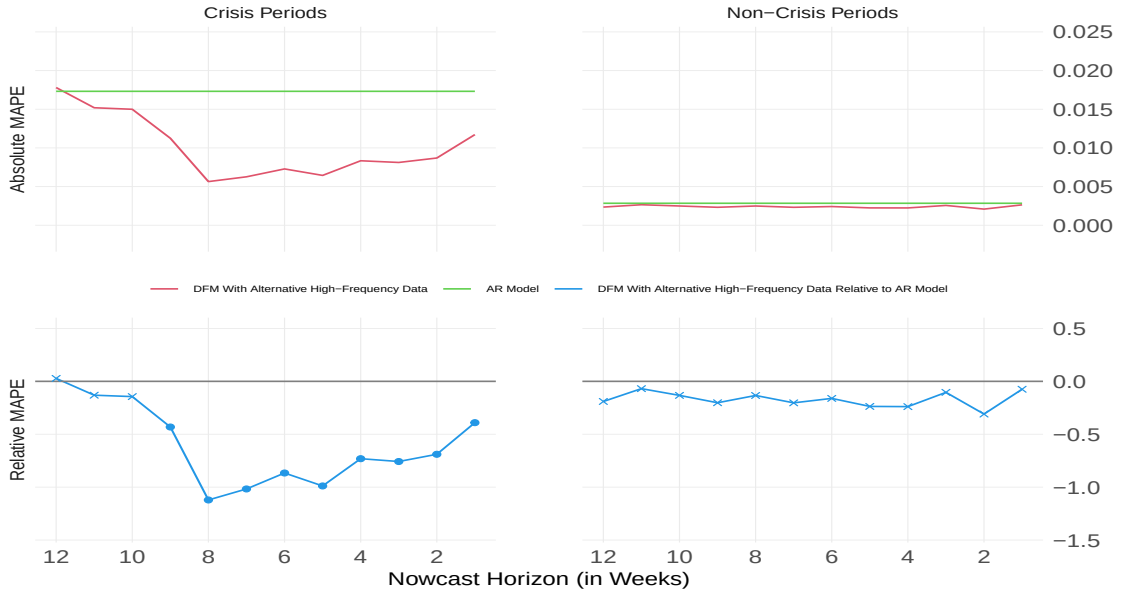

Figure 12: DFM With Alternative High-Frequency Data Against AR Model. Notes: See Figure 7, but MAPEs are displayed instead of RMSFEs.

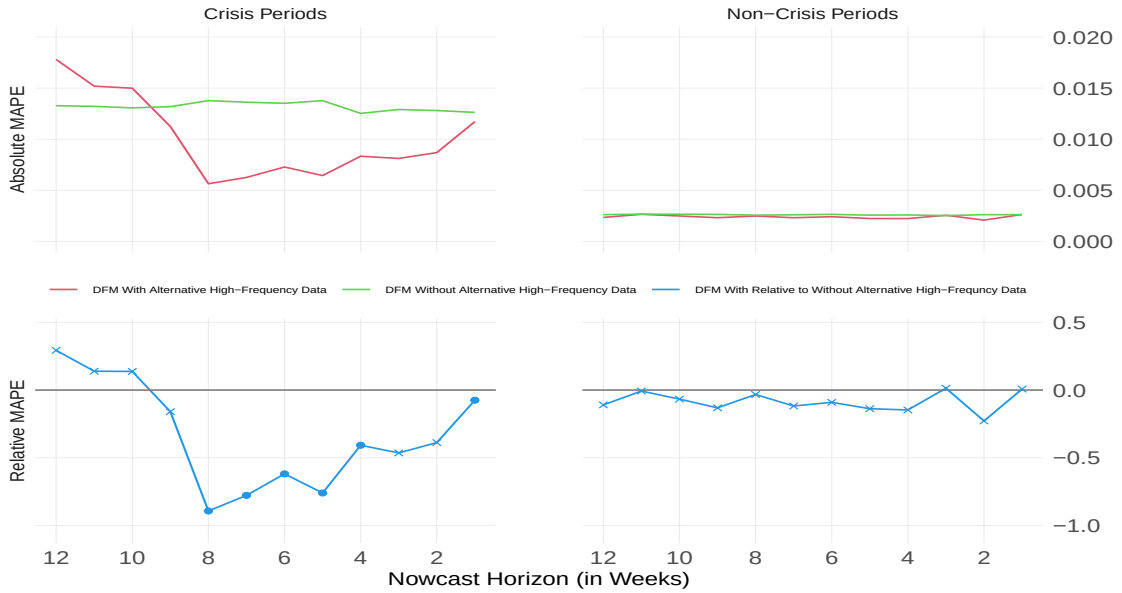

Figure 13: DFM With and Without Alternative High-Frequency Data. Notes: See Figure 7, but MAPEs are displayed instead of RMSFEs.

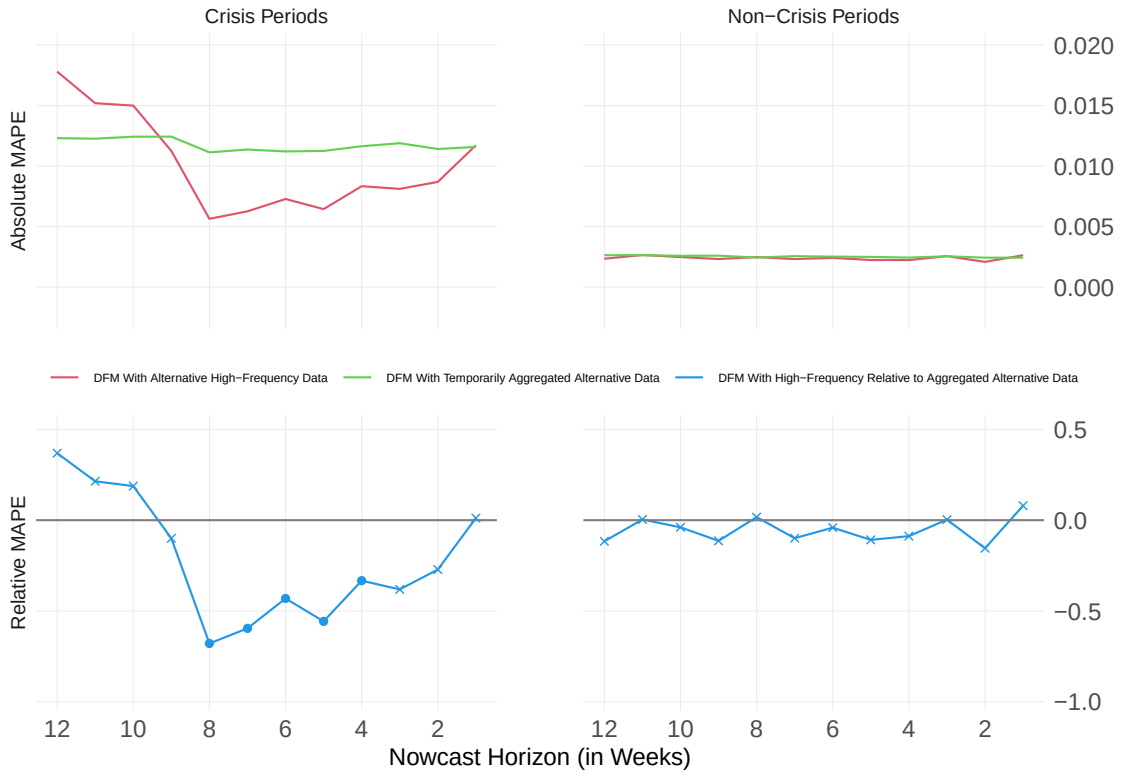

Figure 14: DFM With and Without Temporal Aggregation. Notes: See Figure 7, but MAPEs are displayed instead of RMSFEs.

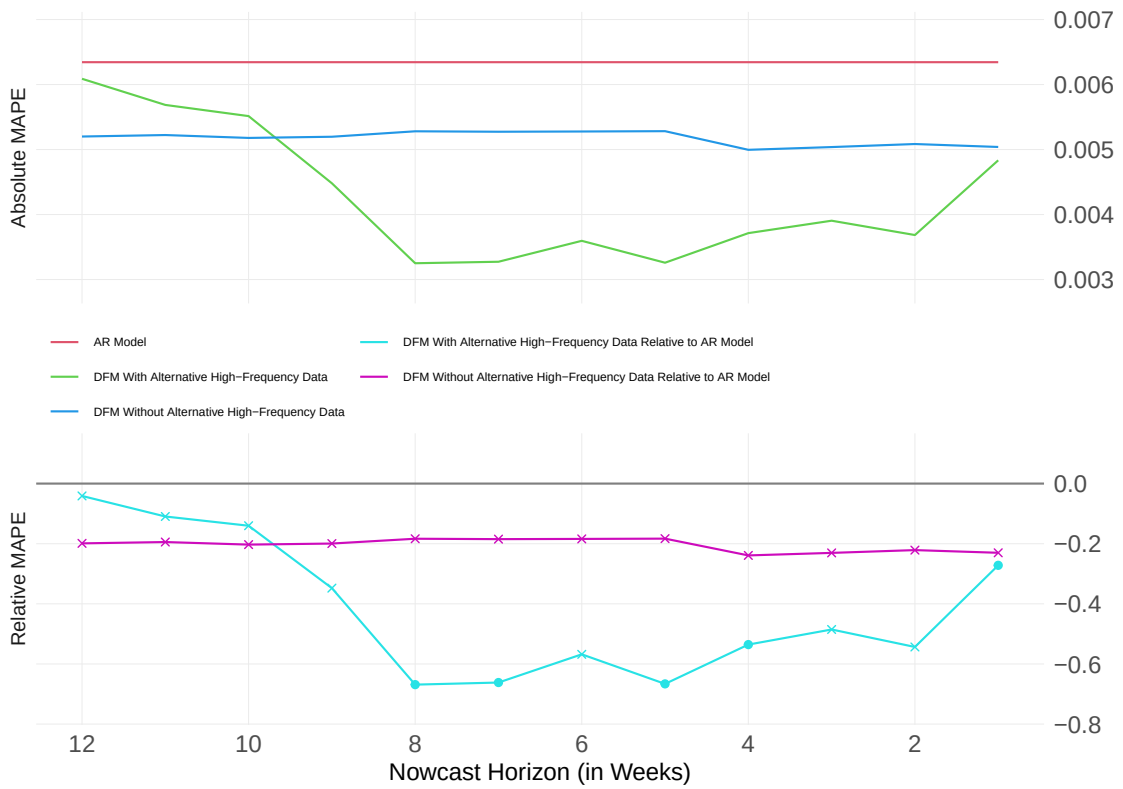

Figure 15: Joint Evaluation of Crisis and Non-Crisis Periods. Notes: See Figure 7, but MAPEs are displayed instead of RMSFEs.

A.8 Accounting for Serially Correlated Measurement Errors

We want to evaluate the usefulness of accounting for serial correlation in the errors of the dynamic factor measurement equation given in Equation (2). For this, we test the significance of the autoregressive coefficients $\rho_1, \ldots, \rho_n$ in Equation (3). We evaluate the marginal posterior distribution of each ρ_i, estimated using the entire data set. It turns out that we can reject, at a 95% significance level, the null hypothesis of ρ_i being equal to zero for 61% of all included variables. In particular, time series with stable trajectories and relatively small innovations, such as interest rates or purchasing manager indices, exhibit highly significant coefficients with magnitudes close to one.

In addition, we estimate the model without accounting for serial correlation in the errors of the dynamic factor measurement equation (i.e. $\rho_1, \ldots, \rho_n$ set to zero) and evaluate the out-of-sample performance. The DFM without accounting for serially correlated measurement errors outperforms the AR benchmark in terms of RMSFE for crisis periods (see Figure 16). This confirms the conclusion in Bańbura and Modugno (2014) that serially correlated measurement errors do not substantially improve the results in terms of RMSFEs. However, the nowcast errors of the DFM turn out to be much more volatile when serial correlation in the factor measurement errors is not accounted for. The differences in the nowcasts errors between DFM and the AR benchmark are therefore not statistically signficant at conventional levels.

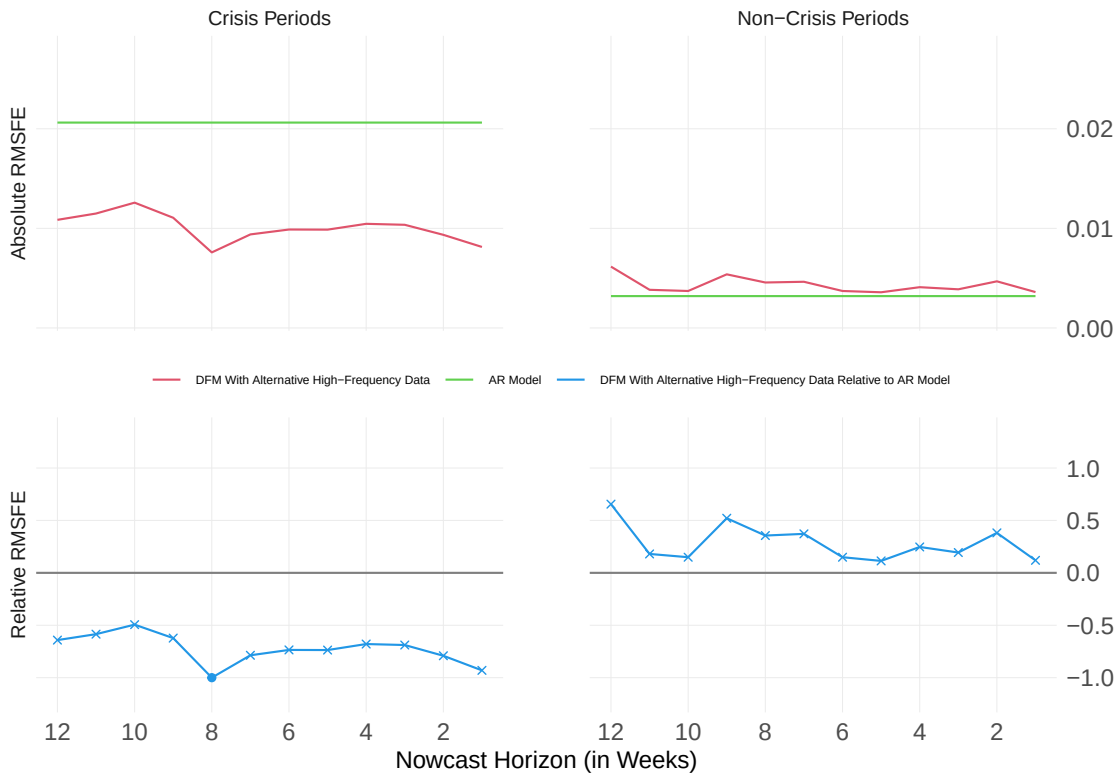

Figure 16: DFM Without Accounting for Serially Correlated Measurement Errors. Notes: See Figure 7.

Further, for non-crisis periods, the DFM performs worse than the AR model in terms of RMSFE, albeit the difference being not statistically signficant. The decreased RMSFE performance is a direct consequence of not allowing for autoregressive processes in the alternative high-frequency data, since these these data then let the weekly GDP indicator become very noisy.

A.9 Declarations

Declarations of interest: None

Authors' contributions: All authors contributed equally to all sections of the manuscript.

Funding sources: No third-party funding has been received.